

# A monitoring system for Sap Flow and Sucrose Measurements in a plant stem

A Thesis submitted to the Faculty of Engineering & Technology,  
Jadavpur University in the partial fulfilment of the requirements  
for the degree of  
Master of technology in  
Instrumentation and Electronics Engineering

Submitted by

RITESH KUMAR THAKUR  
Examination Roll No.: M4IEE1603

Under the Guidance of  
Prof. Kalyan Majumdar

Department of IEE, Jadavpur Univeristy

Department of Instrumentation and Electronics Engineering  
JADAVPUR UNIVERISTY, SALT LAKE, KOLKATA-700098

MAY 2016

Department of Instrumentation and Electronics  
Engineering  
Faculty of Engineering & Technology  
Jadavpur University, Salt Lake  
Kolkata-700098

Certificate of Recommendation

I hereby recommend that the work done by Mr. Ritesh Kumar Thakur (Registration. No. 125094 of 2013-2014) under my guidance, and the thesis entitled “A monitoring system for Sap Flow and Sucrose Measurements in a plant stem” be accepted in partial fulfilment of the requirement for the degree of Master of Technology in Instrumentation and Electronics Engineering from the department of Instrumentation and Electronics Engineering of Jadavpur University.

.....

(Prof. Kalyan Majumder)

Thesis Supervisor  
Department of Instrumentation & Electronics  
Engineering  
Jadavpur University

.....

(Prof. Rajanikanta Mudi)

Head of the Department  
Department of Instrumentation & Electronics  
Engineering  
Jadavpur University

.....

(Prof. Sivaji Bandyopadhyay)

Dean  
Faculty of Engineering &  
Technology  
Jadavpur University

Department of Instrumentation and Electronics  
Engineering  
Faculty of Engineering & Technology  
Jadavpur University, Salt Lake  
Kolkata-700098

Certificate of Approval

The foregoing thesis, entitled as “A monitoring system for Sap Flow and Sucrose Measurements in a plant stem” is hereby approved by the committee of final examination for evaluation of thesis as a creditable study of an engineering subject carried out and presented by Mr. Ritesh Kumar Thakur (Registration. No. 125094 of 2013-2014) in a manner satisfactory to warrant it’s acceptance as a prerequisite to the degree of Master of Technology in Instrumentation and Electronics Engineering. It is understood that by this approval, the undersigned do not necessarily endorse or approve any statement made, opinion expressed or conclusion drawn therein, but approve the thesis for the purpose for which it is submitted.

Committee of final examination for evaluation of thesis:

.....  
(Signature of Examiner)

.....  
(Signature of Supervisor)

# Declaration of originality and compliance of Academic Ethics

I hereby declare that this thesis contains literature survey and original research work by the undersigned candidate, as a part of his Master of Instrumentation & Electronics engineering studies.

All information in this document have been obtained and presented in accordance with academic rules and ethical conduct.

I also, declare that as required by these rules and conduct, I have fully cited and referenced all material and results that are not original to this work.

Name:

Roll Number:

Thesis Title:

Signature with Date:

## Acknowledgements

This thesis becomes a reality with the kind support and help of many individuals. I would like to extend my sincere gratitude to all of them.

First of all, I would like to express my deepest gratitude to my project guide **Prof. Kalyan Majumder** for his valuable support in providing resources, insights and advices during my project work. I must mention that this thesis would not have been completed without his constant support and encouragement despite of his busy schedules.

I take immense pleasure to express my gratitude to **Prof. Rajanikanta Mudi**, Head of the Department of IEE.

I would also like to express my gratitude to **Mr. Sunil Dutta** for their valuable advices and assistance during my project work.

It's my pleasure to express my thankfulness to Soumyadeep Datta, Saurabh Animesh, students of IEE., Jadavpur University for their valuable suggestions throughout the work. I would like to confess my heartily gratitude to the Teaching and Non-Teaching staff of Dept of IEE for providing required equipments, devices and whatever help they have given.

Also, I would like to thanks my beloved **Mama Jee** for his constant support and motivation to pursue my academic career and I must admit that without his continual support I wouldn't have been here writing this project.

Last but not the least, a word of thanks goes to my loving **family** for their immense support throughout my academic career and I am very much thankful to all of my classmates, my friends for their support and encouragement.

.....

(Ritesh kumar Thakur)

Instrumentation & Electronics Engineering  
Jadavpur University

## Motivation

This project work has been done for supporting the actual project, whose objective is to “develop resilient rice varieties for drought prone environments” sanctioned by Indian council of agriculture research (ICAR). Therefore, in the present work our first aim was to calibrate the sap flow sensor so that it can be employed into the rice plant for the measurement of minimal requirement of water for surviving into drought prone environments. For that reason, we have made an attempt to calibrate the sap flow gauge on a measurement set-up referred as virtual plant model. Sap flow gauge is a very powerful sensor for measuring plants and crops water use. It measures the direct mass flow rate of the water flowing through the stem of the plants. It is widely employed in the field of agriculture. It is used to investigate agronomical and hydrological outcomes of the plant. Observing the sap flow, it may help us to monitor the health of the plant, root damages and insect damages.

The second part of this work is also a part of project “development of sucrose sensor for phenotyping of soil moisture-deficit stress tolerance in rice” sanctioned by Indian council of agriculture research (ICAR). Therefore, to measure the sucrose content from the plant stem we are going to use a novel method known as “low power continuous wave (CW) excitation Raman spectroscopy”. This method has many advantages over other methods such as, no sample preparation needed, this method is non-destructive, the measurements can be performed in a very short detecting time (i.e., on the order of several seconds as opposed to several minutes) and the major advantage of this technique is that it may be applied both in vivo and in vitro experiments, because this technique doesn't require much power to perform the experiments which may destroy or burn the biological sample.

## Abstract

The present work describes about “A monitoring system for Sap Flow and Sucrose Measurements in a plant stem”. Therefore, in the first part of the work, we have described about the measurement and analysis of the sap flow in the stem of the virtual plant model using the sap flow sensor. The sensor which we have used is based on the method “Stem Heat Balance Theory”. However, to analyse the results for our experiments, there is no such reference data or any tool available to us. Therefore, to test our experimental results, we have made an attempt to develop such a measurement set-up which can be used to analyse the experimental results directly without any reference data and the sap flow sensor may be calibrated without making any great effort. The measurement set-up which we have made is referred as virtual plant model. Also, to improve the accuracy of the results, we have made several configurations of the virtual plant model. However, in the present work, we have only included a few configuration of the virtual plant model which could be appreciated up to some extent.

The second part of this work describes about the measurement of sucrose content by low power continuous wave Raman spectroscopy. This method is applicable for both qualitative and quantitative measurements. This method requires a tuneable laser which is very costly. But we are only interested in quantitative measurements and therefore we have proposed a measurement set-up that doesn't require the tuneable laser. The proposed measurement set-up can be applied to quantitative measurements of any biological sample if the Raman shift of the biological sample is known in advance.

# Contents

## 1 Introduction and Literature Review

1.1	Sap flow measurements .....	1
1.2	Theory .....	3
1.3	Gauge design .....	5
1.3.1	Dynamic response .....	5
1.3.2	Applications .....	6
1.3.3	Examples of species .....	7
1.3.4	Systems for monitoring sap flow .....	7
1.4	Measurement of sucrose .....	9
1.4.1	Sucrose Measurement techniques .....	11
1.5	Raman spectroscopy .....	13
1.5.1	Conventional Raman effect .....	13
1.5.2	Dispersive Raman spectroscopy .....	15
1.5.3	FT- Raman spectroscopy .....	15
1.5.4	Low power CW excitation Raman spectroscopy ...	17
1.5.5	Working principle of low power Raman spectroscopy .....	19
1.5.6	Measurement of sucrose by low power CW Raman Spectroscopy .....	21
1.5.7	Working principle of proposed low power CW Raman spectroscopy .....	23



## **CONTENTS**

1.7	Objective and organization of thesis .....	25
-----	--	----

### **References**

## **2 Virtual Plant Model (VPM) 30**

2.1	Theory of the sap flow meter .....	30
2.2	Sap flow meter specifications and its body construction .....	31
2.3	Electrical specifications .....	31
2.4	Sap sensor construction .....	33
2.5	Design of the virtual plant .....	33
2.5.1	Syringe infusion pump (LPM-50DN) .....	34
2.5.2	PVC pipe .....	34
2.5.3	Medical syringe and virtual plant model .....	35
2.6	Design of the amplifier .....	36
2.6.1	Operational amplifier (AD 8630) .....	36
2.6.2	Amplifier circuit diagram .....	37
2.7	Stem heat balance theory and working equations .....	37
2.7.1	Working equations .....	38
2.7.2	Sap thermodynamics equations .....	39
2.7.3	Apparent $K_{sh}$ calculation .....	40
2.7.4	Steps to be followed to compute flow rate F .....	40

## **3 Experiments 41**

3.1	Experiment number 1 .....	41
3.1.1	Results and discussions .....	43
3.2	Experiment number 2 .....	44

## ***CONTENTS***

3.2.1	Results and discussions .....	44
3.3	Experiment number 3 .....	45
3.3.1	Computation of the flow rate F .....	45
3.3.2	Calculation of sheath conductance .....	46
3.3.3	Results and discussions .....	47
3.4	Experiment number 4 .....	50
3.4.1	Calculation of sheath conductance .....	51
3.4.2	Results and discussions .....	53
<b>4</b>	<b>Conclusion and Future scope</b>	<b>56</b>
4.1	Conclusions .....	56
4.2	Future scope of the work .....	57
<b>APPENDIX</b>		
A-1	Dynagage Sensor Installation (with weather shield) .....	58
A-2	Sensor Maintenance .....	59
	<b>References</b>	<b>60</b>

# List of Figures

1.1	Heat balance of the heated stem system. Where $Q_s$ is the rate of heat transport by the sap stream .....	3
1.2	Vertical cross-section of a stem with a gauge in place .....	3
1.3	Flow 32 Sap Flow System .....	8
1.4	An overview of 32 Dynagage System .....	8
1.5	Applications of sucrose .....	9
1.6	Synthesis of sucrose from glucose and fructose, and their respective chemical structures .....	10
1.7	Overview of conventional Raman effect .....	13
1.8	Energy level diagram .....	14
1.9	Pump laser signal and scattered spontaneous Raman signal .	18
1.10	Irradiated probe signal .....	18
1.11	Enhanced Raman signal .....	19
1.12	Schematic of the low-power CW Raman spectroscopy.....	20
1.13	Raman spectra of the sucrose solution at 24 & 66% (w/w) concentration .....	22
1.14	Schematic of the proposed low-power CW Raman spectroscopy .....	22
2.1	Schematic of Dynagage sap sensor .....	30
2.2	Construction of Dynagage sensor and female connector Model	33
2.3	Syringe infusion pump .....	34
2.4	PVC pipe of 5 mm diameter .....	34
2.5	5 ml Syringe and Virtual plant model .....	35

## ***LIST OF FIGURES***

2.6	AD8630 TOP VIEW .....	36
2.7	Non-inverting Amplifier .....	37
2.8	Stem Gage Schematics .....	37
2.9	Thermocouple and heater in Dynagage .....	38
3.1	See how the sensor is installed in the stem of virtual plant model for performing the experiment .....	42
3.2	Sap-flow rate analysis .....	48
3.3	Change in temperature versus Flow rate .....	49
3.4	Heat flux analysis .....	49
3.5	Sensor installation in the vertical direction .....	50
3.6	Sap-flow rate analysis .....	53
3.7	Change in temperature versus Flow rate .....	54
3.8	Heat flux analysis .....	54
3.9	Calibration curve for the experiment no. 4 .....	55

## List of Tables

1.1	Flow gauge applications .....	6
1.2	Example of the species .....	7
1.3	Assignment of the frequencies observed in the spectra of the sucrose in aqueous solutions .....	22
2.1	Mechanical Specifications .....	31
2.2	Heater input voltage .....	32
2.3	Heater input power .....	32
2.4	Heater impedances .....	32
3.1	Readings taken in the interval of 30 minutes using 20 ml syringe on 2nd march 2016 .....	41
3.2	Readings taken in the interval of 30 minutes using 20 ml syringe on 3rd march 2016 .....	43
3.3	Readings taken in the interval of 30 minutes using 20 ml syringe on 8th march 2016 .....	43
3.4	Readings taken in the interval of 30 minutes using 5 ml syringe on 9th march 2016 .....	44
3.5	Readings taken in the interval of 30 minutes using 20 ml syringe on 10th march 2016 .....	45
3.6	Actual flow rate versus measured flow rate .....	46
3.7	Error between actual flow rate and measured flow rate .....	47
3.8	Readings taken in the interval of 30 minutes using 20 ml syringe on 6th April 2016 .....	51
3.9	Actual flow rate versus measured flow rate .....	52
3.10	Error between actual flow rate and measured flow rate .....	52

# Chapter 1

## Introduction and Literature Review

This thesis contains two main parts: the first part is about sap flow measurements and second part is about measurement of sucrose content by Raman spectroscopy. Therefore, in this chapter, we will first talk about the sap flow measurements, its theory in brief, gauge design, dynamic response of the gauge and sap flow application. Thereafter, in the second part, we will talk about sucrose measurement techniques, conventional Raman effect, dispersive Raman spectroscopy, FT- Raman spectroscopy, and the limitations of these techniques and to overcome these limitations, we will talk about low power continuous wave (CW) excitation Raman spectroscopy and then we will see the proposed method for the measurement of the sucrose content.

### 1.1 Sap Flow Measurements

Sap flow measurements provide us a powerful tool for the study of plant water relations and monitoring qualitative physiological responses of plants to environmental conditions. Sap flow methods are widely employed to investigate the agronomic, ecological and hydrological outcomes of plant growth. Adding heat to the moving sap of plants as a means of measuring the sap flux is not new. Huber's work [1] in 1932 laid the foundation for what is currently known to as the heat pulse velocity (HPV) technique. In this heat pulse velocity method, the sap velocity is estimated from the time required for a heat pulse, injected into the xylem, to travel a finite distance downstream. Bloodworth [2], Closs [3], Swanson [4], Lassoie [5], Miller [6], and Cohen [7] have contributed to heat pulse velocity theory and technique. The limitation of this method was to measure only the sap velocity. Calculation of sap flux (mass  $\times$  time) from the sap velocity requires a knowledge of the active conducting area of the xylem, a figure difficult, if not possible, to obtain, and not constant over time. Hence, the heat pulse velocity technique requires an empirical and variable conversion factor obtain by recording the rate of water loss by weighing.

Numerous sap flow measurement techniques have been developed to continuously improve the quality of the measurement and to quantify volumetric water use in plants with great accuracy. Several scientific research institutions worldwide conducted many years of cooperative research and development on the heat stem-flow technology. A direct measurement of the mass flow of the sap with a stem heat balance (SHB) technique, using a continuous application of heat, was first proposed by Vieweg and

Ziegler [8], and later by Daum [9]. This last approach draws up a heat balance for a stem segment supplied with a known amount of heat,  $P$

$$C_{st} \frac{dT_{st}}{dt} = P - Q_r - Q_u - Q_d - Q_c \quad (1)$$

Heat (in W) is lost from the segment by conduction (radial heat loss,  $Q_r$  and heat loss in the downstream and upstream directions,  $Q_d$  and  $Q_u$  respectively), and  $Q_c$  is the convection in the sap stream. The left hand term in the equation represents the change in heat storage within the segment;  $C_{st}$  is the heat capacity ( $J K^{-1}$ ) and  $T_{st}$  the average temperature of the stem segment (in K) and the heat transported by sap mass flow  $Q_c$  is given by

$$Q_c = C_w F (T_d - T_u) \quad (2)$$

Where  $C_w$  is the specific heat of sap (taken as that of water because approx 99% sap content is water),  $F$  is the mass flow rate of water ( $gm h^{-1}$ ), and  $T_d - T_u$  is the difference in the temperature of water entering and leaving the heated segment. If  $Q_c$  can be evaluated, and  $T_d - T_u$  measured, then the mass flow rate of water,  $F$ , through the stem can be computed directly.

This approach has been applied in two different techniques. The first, where large heaters are implanted into the stem, was suggested by Daum [9] and was developed by Cermak and colleagues [10, 11] and is suitable only for larger stems. A second, non-invasive technique that is suited for both medium and small stems uses an insulated flexible heater wrapped around the stem, and temperature sensors (especially thermocouples) to measure conductive fluxes. Two techniques have been suggested using this later approach. One uses a steady-state assumption (assuming the left hand in Eq. (1) is zero, with a constant power input through the heater, following the work of Sakuratani [12, 13] and the subsequent development by Baker and Van Bavel [14] and Steinberg [15]. The other technique (technically more difficult) uses a variable power input to maintain the temperature difference between a reference point in the heated stem and the air constant [16]. The advantage is that the dynamic response of the gauge is independent of the flow rate and hence this method is therefore more accurate.

Since gauges became commercially available in the late 1980s, the steady-state method has been used on a wide variety of both herbaceous (e.g., tomatoes, potatoes, sunflower, cotton, maize sugarcane) and tree (e.g., coffee, peach, pecan, hibiscus, roses, mesquite, vines) species. The magnitudes of the errors owing to gauge design and measurement

resolution have been analyzed in great detail elsewhere [12, 13, 17, 18]. However, the basic assumption that steady-state conditions exist has not been considered in detail, except by Groot and King [17] who considered in particular the low flow rate conditions in confiner seedlings. The importance of stem temperature changes will depend on sap flow rate, and on stem size, Groot and King [17] noted that at low flow rates it was essential to include the heat storage term in the computation of sap flow rate. Dugas [19] working with cotton, found the heat storage term insignificant, but Shackel [20] working with large-diameter peach, found it on occasion so large as to invalidate their estimates of flow rate.

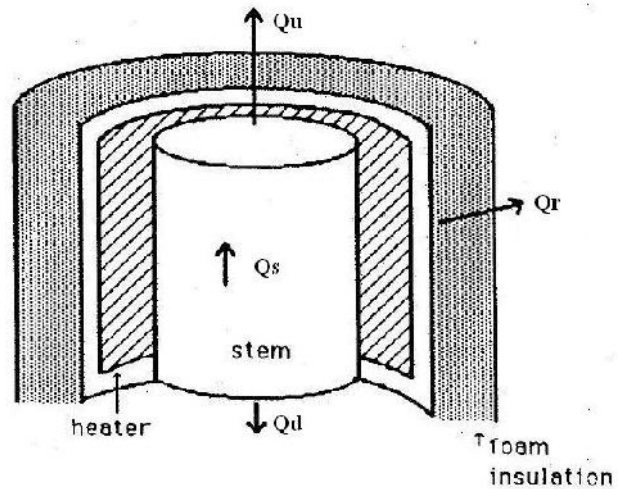


Figure 1.1: Heat balance of the heated stem system. Where  $Q_s$  is the rate of heat transport by the sap stream.

## 1.2 Theory

The heat balance approach proposed by Sakuratni [12] can be described with reference to Fig 1.1. A flexible heater encircles the stem and provides a small, steady and known amount of heat. Insulation, with a thermal conductivity much lower than that of plant tissue, encloses the heated segment and extends for several centimeters both above and below it. In the steady state, the continuous heat must be balanced by the heat flow out of the system, the system being composed of the heated segment and the heater. The outward heat flow can be partitioned into conductive fluxes up and down the stem, radial conduction into the insulation and mass heat transported by the sap stream, whatever its direction and however distributed over the cross-section.

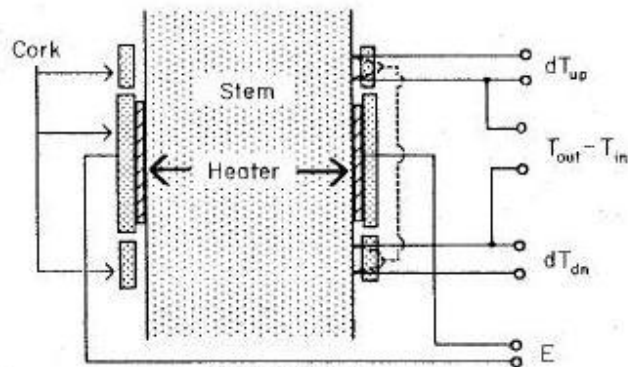


Figure 1.2 vertical cross-section of a stem with a gauge in place.



Figure 1.2 illustrates how each of the heat fluxes is measured. The conductive flux of heat upwards ( $Q_u$ ) can be calculated with Fourier's law for a one dimensional heat flow (see Eq. 1.1)

$$Q_u = k_{st} A \frac{dT}{dX} \quad (\text{W}) \quad (1.1)$$

Where  $k_{st}$  is the thermal conductivity of the stem tissue (W/(m·K)),  $A$  is the cross-sectional area of the stem (in  $m^2$ ), and  $dT/dX$  is the temperature gradient (in K/m). The derivative in eq. (1.1) is approximated as the output from two differentially wired thermocouples which were 3 mm apart and in direct contact with the stem, the lower of the two being immediately above the heater. This presumes, as was done by Sakuratani [12] that owing to the radial and vertical extent of the insulating jacket, the gradient of the temperature was uniform over the cross-section. Another pair of thermocouples located similarly below the heater allowed the determination of the conductive flux downward. In eq. (1.1), the value of  $A$  must be known from an actual measurement, and that of  $k_{st}$  is taken to be .54 W/(m·K) a value which is the average of measured values reported for various stem of the herbaceous plants [13] and is slightly less than that of water.

The radial outward flow of heat is calculated from the voltage output of a thermopile composed of eight thermocouples in series, located on either side of a 2 mm cork sheath between the heated and the foam insulation. The flux is approximated by eq. (1.2), the integrated form the equation for radial heat flow ( $Q_r$ ) in a cylinder of infinite length [21]

$$Q_r = 2\pi K_{co} L (T_i - T_o) / \ln(r_i / r_o) \quad (\text{W}) \quad (1.2)$$

Where  $K_{co}$  is the thermal conductivity of cork (W/m·K),  $L$  is the length of the heated segment (in m),  $T_i$  is the temperature at the inner surface of the sheath (K),  $T_o$  is the temperature at the outer surface of the sheath (K),  $r_i$  is the radius of the inner surface of the sheath (m), and  $r_o$  is the outer surface of the sheath (m). All the parameters in eq. (1.2) are constant for a given configuration, and can be combined with the conversion factor relating the thermopile output (E) to the temperature difference ( $T_i - T_o$ ), into a single sheath conductance,  $K_{sh}$  with units of W/V<sub>o</sub> (the subscript signifying voltage output from the thermopile), so that eq. (1.2) may be equivalently written as

$$Q_r = K_{sh} E \quad (\text{W}) \quad (1.3)$$

Subtraction of the three heat fluxes (up, down, radial) from the known heat input gives the heat transported by the sap stream. To compute the mass flow rate of the water from the sap heat transport, it is necessary to know the temperature difference between the

water entering and leaving the heated portion of the stem. To obtain this value, the thermocouples nearest the heater are differentially wired to the lower nearest the heater. Again, the assumption of radial thermal homogeneity is made. This temperature difference, multiplied by the heat capacity of water, is divided into the sap heat transport, yielding the mass flow rate of the sap itself.

$$Q_c = \frac{P - Q_r - Q_u - Q_d}{C_p (T_d - T_u)} \quad (\text{g/sec}) \quad (1.4)$$

Where  $Q_c$  is the computed sap flow rate (g/sec),  $P$  is the power input to the heater (W),  $C_p$  is the heat capacity of the xylem sap (J/(g·sec)),  $T_d$  is the temperature of the junction below the heater (K), and  $T_u$  is the temperature of the junction above the heater (K).

**The value of  $K_{sh}$ , in eq. (1.3), is calculated from the eq. (1.4), by setting  $Q_c$  equal to zero** and making measurements on a stem that has been excised and sealed with vaseline, to ensure that sap flow rate is zero. This procedure is a zero set, not to be confused with a calibration or measurement of the response to known changes in sap flow rate. In this sense (and in contrast with most transient techniques), the method is absolute.

## 1.3 Gauge Design

Baker and Van Bavel [14], tested four gauges, designed by Sakuratani [12,13] and fabricated as described by him. Their testing results showed each gauge accurate to within  $\pm 10\%$ , but they have encountered two problems. First, the manganin wire used to make the heaters was susceptible to corrosion. In continued use, three of the gauge's heater lost continuity, a problem Sakuratani [12] had also noted. The second problem was the fragility of the thermocouples, which tended to break loose from their backing or to pull away from direct contact with the stem, particularly during the process of installing or removing the exterior foam insulation sheath. These problems were modified by Baker and Van Bavel [14] and they have designed the improved version of the earlier gauges.

### 1.3.1 Dynamic Response

The method requires the establishment of a steady-state, so there is always a lag in the response of the gauge to sudden change in stem flow, due to the thermal inertia of the stem. The time constant of such a system was given by Kucera, Cermak & Penka [22] as

$$\dagger_c = \frac{m_s \times C_{p,s}}{Q \times C_{p,w} + L_s} \quad (1.5)$$

Where  $\tau_c$  is the time constant (sec),  $m_s$  is the mass of the heated segment (kg),  $C_{p,s}$  is the heat capacity of the segment (J/(kg·K)),  $Q$  is the stem flow rate (kg/s),  $C_{p,w}$  is the heat capacity of xylem sap (J/(kg·K)) and  $L_s$  is the thermal conductance of the system (W/K). The last quantity is the rate of heat loss at zero sap flow rate for each degree of temperature difference between the heated segment and its environment.

It can be seen from eqn. (1.5) that the dynamic response of the system can be improved by either reducing the size of the heated segment or increasing the thermal conductance of the system, but there are practical limitations in both cases. In particular, if the heated segment is made too small, the heat input power must also be reduced to avoid physiological damage, with the result that the various outward fluxes and the corresponding signals also diminish increasing the relative error of the measurement. If the thermal conductance of the gauge is made too large, the assumption of one-dimensional conduction in the stem becomes increasingly tenuous.

## 1.3.2 Applications

The sap flow gauge has a large applications and it can be applied in many fields. The following applications have been shown below.

Table 1.1: Flow gauge applications

Agriculture Engineering	Hydrology
Agriculture Consultant	Irrigation Systems
Botany	Orchard Monitor
Citrus Grower	Ornamentals Farm
Crop science	Plant Physiologist
Crop physiology	Pollution Studies
Extension Service	River Authority
Fertilizer Evaluation	Reforestation
Generic Engineering	Seed Genetics
Greenhouse Control	Tree farm
Farm Industry	Forestry Company

### 1.3.3 Example of Species

These are the examples of the species that have been monitored successfully by Dynagage technology.

Table 1.2: Name of the species

<b>CROPS</b>	<b>TREES</b>	<b>OTHER</b>
Cucumber	Almond	Ligustrum
Cotton	Loblolly Pine	Mesquite
Corn	Bald Cypress	Rubberplant
Sorghum	Red Cedar	Rose
Sunflower	Oak	Grape
Sugarcane	Douglas Fir	Fruit Peduncles
Sweet potato	Willow	Stomatal
Tomato	Peach	Oscillations
Potato	Pecan	Mangosteen
soybean	Pine	Coffee

### 1.3.4 Systems for Monitoring Sap Flow

Dynamax Inc. through Irricrop Technologies Ltd in Narrabri, developed this Irrigation Symposium widely known as Flow32 system. Flow32 integrates all of the logging, storage, retrieval, and power functions into a complete package (see fig 1.3). IBM PC portables or compatibles are the best choice to load programs and to run formatting or retrieval utilities. The system includes multiplexers, assembled and tested wiring, a solar panel or 120V power supply, voltage regulators, retrieval cables, data storage modules, weather proof enclosures. Dynamax therefore designed the system to not only include all of these functions, but to incorporate real-time graphics for environmental control chamber and glasshouse monitoring. The use of menus and other simple software tools were integrated into a fully assembled package which makes system initialization and starting to gather data a much simple task. Most importantly, the system will collect data from one to 32 Sap flow sensors simultaneously. An initial system comprising five sensors and all of the software, the controller, DNX10, and retrieval modules, is called the Flow32-A. As shown in the fig. 1.4 (see in the next page), the system can be

economically expanded in modules of eight sensors per multiplexer. The Flow32 sap flow system is a controller/datalogger is a special version of CR10 that also retains its general purpose data collection functions.

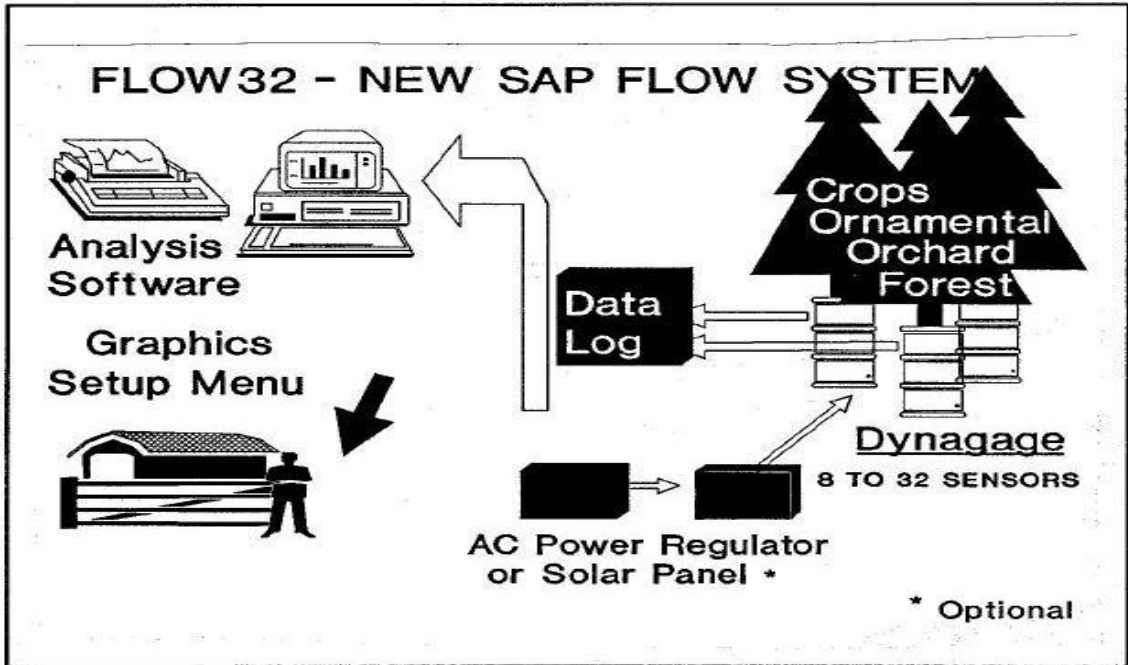


Figure 1.3: Flow32 Sap Flow System

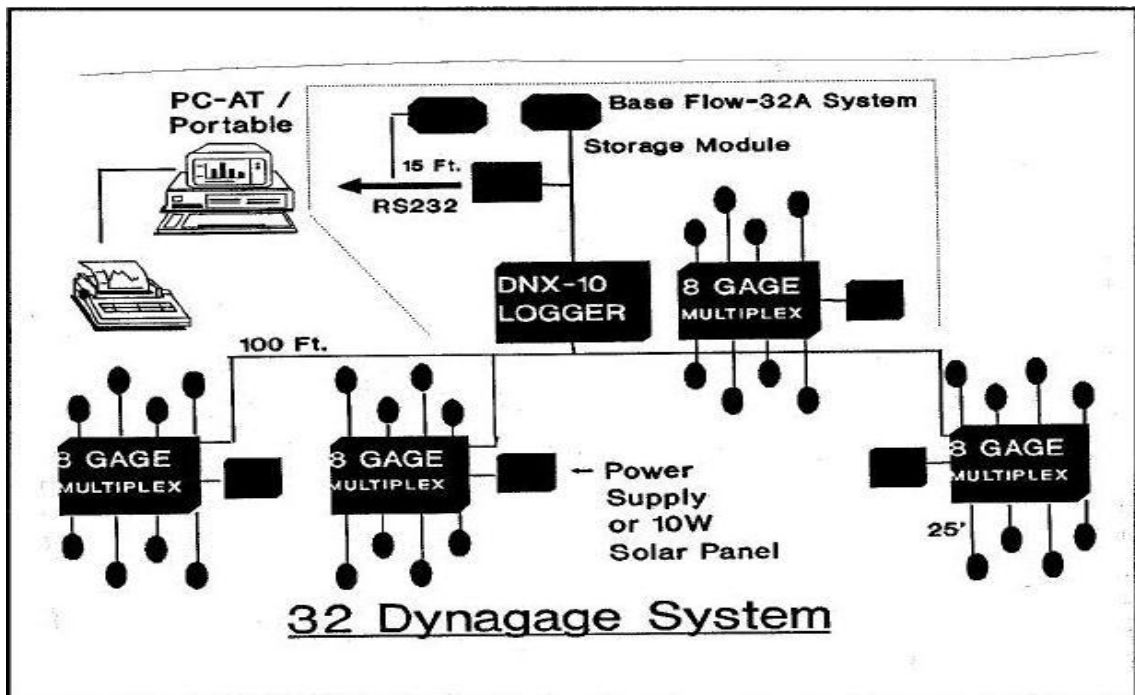


Figure 1.4: An overview of 32 Dynagage System

## 1.4 Measurement of Sucrose

Sucrose is one of the most abundant organic compounds produced in the world. It is easily available at very low cost with very high level of purity. It is synthesized by almost every green plant and is assimilated by most organisms. One of the main natural resources of the sucrose is the Sugarcane that may contain from 14% to 24% v/v of sucrose and the other popular natural resource is the sugar beet. Sugarcane and the sugar beets serve as the major storage of saccharides. In other plants, it is converted to starch, inulin, or levan for carbohydrate storage. In many plants, the transport of oligo and polysaccharides from one part of the plant to another proceeds through conversion to sucrose, translocation, and resynthesis. Modern sugar industries produce a white, odorless, crystalline powder with a sweet taste of pure sucrose, devoid of vitamins and minerals via the process of bleaching and crystallization. This refined form of sucrose is usually known as table sugar or just sugar. According to “Sugar: world Markets and Trade [24]” sucrose sugar were produced about 175 million metric tons worldwide in 2013. It plays a central role as an additive in food production and food consumption all over the world.

Sucrose is one of the major international agriculture products. It is widely used in the beverage and food industries. It has a large application in confectionary and as a sweetening ingredient. With sufficient concentration it can be used as a food preservative in jams, processed food, and condensed milk. All processed sugar that is commonly used in homes and industries actually comes from sugar cane and sugar beets. Sucrose is also used in the chemical and processing industries. An industrial chemical process based on sucrose must convert sucrose into conventional feedstock, such as ethanol and ethylene products that utilize the particular properties of the sucrose molecule. Along these sucrose is used in the cellulose industry, and also in the manufacture of ink.

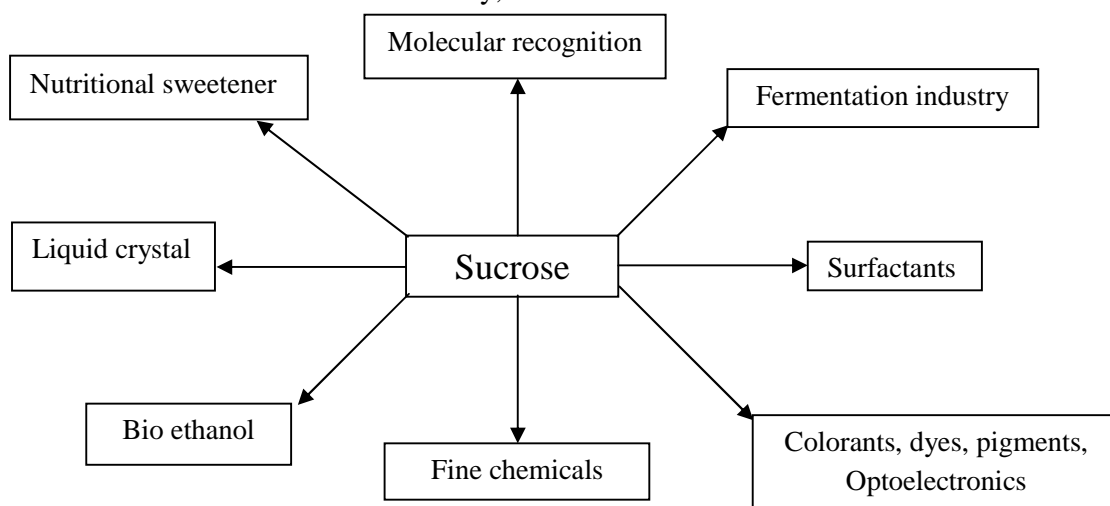


Figure 1.5: Applications of sucrose

There is also a huge demand of sucrose in large-volume markets such as surfactants, plastics, and polymers. It is a very useful product for pharmaceutical application. The utilization of sucrose in food and other industries is illustrated in the Fig. 1.5. Structurally, the sucrose is a disaccharide constituted by the union of the monosaccharides glucose and fructose, connected through their anomeric carbons and constitutes the molecular formula  $C_{12}H_{22}O_{11}$ . The molecular structures of glucose, fructose, and sucrose are illustrated in Fig. 1.6.

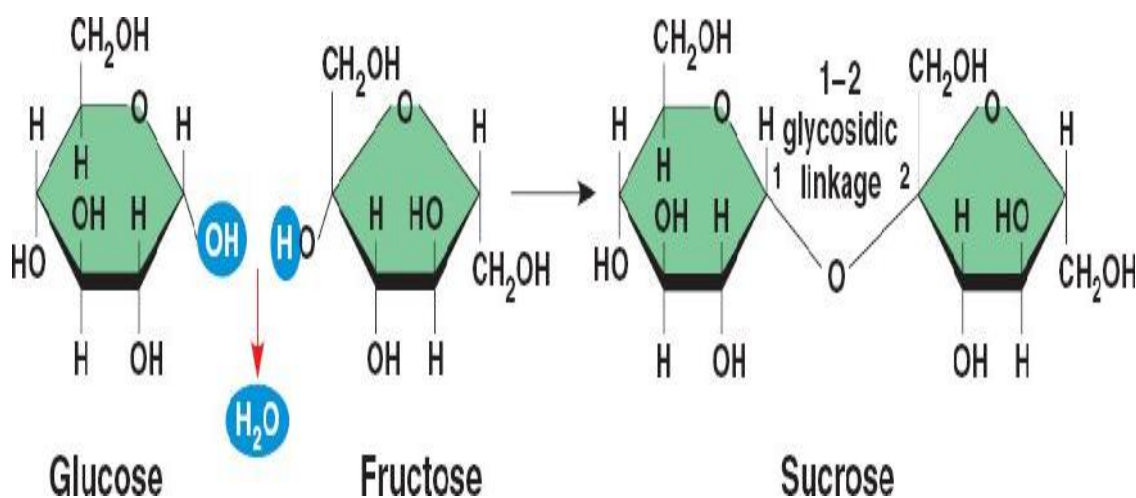


Figure 1.6: Synthesis of sucrose from glucose and fructose, and their respective chemical structures.

We know that sugar is the main product of the sucrose and it is largely employed in industrialized food in order to control the acidification during food processing, aiming to conserve and to change the acid taste of natural foods as milk and fruits [25]. The addition of excessive quantity of sugar transforms the food in a calorie bomb with eventual pathogenic effect [26]. The increase in the consumption of calories from carbohydrates has been positively correlated with the alarming rise of the “metabolic syndrome” [26, 27]. Recently, it was shown that the overload of fructose in the diet of male mice during two months, despite of no induced changes in blood glucose and insulin baseline, resulted in impaired glucose tolerance [28]. With the regular, non-diet/light soft drinks, this biochemical phenomenon is not different as function of the high amount of sugar added and it is highly consumed by general population [25, 29] and dangerously by the ingestion in childhood and adolescent, which could cause increased obesity risk in adulthood [30]. It was also demonstrated that highest concentration of carbohydrates in the diet, especially in its simplest form, constitutes a substantial risk factor for the development of obesity and diabetes [29].

As we have seen that sucrose is used for many purposes and the measurement of sucrose is a routine activity in the food industries, and if the content of sucrose is altered from the desired content then it can create a lot of problems as said above. Therefore, monitoring the purity of the sucrose in the food products at the time of food processing is very important and hence, the need of the measurement of the sucrose content is of a great interest.

### **1.4.1 Sucrose Measurement Techniques**

The simplest way of the sucrose measurement method for industrial purpose is by taking and optical rotation measurement with a Polarimeter. In this measurement the system will bring the sample to a specified temperature and when the sample is stable at that require temperature it will measure the optical rotation and display the concentration of the sample. This is the standard method of the sucrose measurement in the process analytical technology. Process analytical technology works on the principle of implementing quality into the product at the time of manufacturing. This concept actually aims at understanding the process by defining their Critical Process Parameters and accordingly monitoring them in a timely manner (preferably real-time monitoring) and thus being more efficient in testing while at the same time reducing over-processing, enhancing consistency and minimizing rejects.

One of the methods of investigating the sucrose and glucose level is to use the biosensor. Biosensors are analytical instruments that couple an analyte-specific enzyme with an electrochemical detector [31]. When the target molecule interacts with the enzyme, the electrochemical detector detects the interaction and subsequently determines the concentration of the target molecule. The most commonly known biosensor is the glucose dehydrogenase (GD) biosensor which is used by diabetics to monitor blood glucose concentration. The GD biosensor specifically targets glucose and is an important biosensor for the sugar industry as the GD biosensor is, at this point in time, the only biosensor able to measure sugars via intermediate reactions involving glucose. Biosensors offer a very cheap, rapid and reliable means of selectively measuring glucose [31] and can be adapted to measure sucrose by the addition of invertase into the analytespecific enzyme layer [36].

The GD/invertase multiple enzyme system has many complications including the instability of enzymes (particularly invertase [32]), incompatible pH and temperature ranges for the different enzymes and the degradation over time of electrodes [33, 34, 35]. There has also been research involving a flow injection system where enzymes are successively added. However, problems with pH and enzyme stability still arise while the hardware becomes more complex [36]. Routine measurement techniques currently used by the sugarcane industry to measure or infer sucrose concentrations are refractive index, density and polarimetry All of these techniques axiomatically calculate the amount of



sucrose using empirical rules. These approaches have been adopted due to the significant capital expense and specific laboratory expertise required at sugar mills and small research centers to operate high performance liquid chromatographic (HPLC) methods which are capable of accurately measuring specific sugar concentrations.

The other conventional methods, such as gravimetric, titulometric and spectrophotometric techniques, together with the HPLC with refraction index detector have been widely employed in industries [37]. These conventional methods such as gravimetric and titulometric methodologies, are still applied in spite of the tedious character of these procedures. Furthermore, these methods require great quantity of reagents, implying that in a determined interval of time, these analytical procedures represent a very higher cost to the factories as compared with some spectroscopic alternatives [38]. These analytical procedures are also very time consuming as compared to the spectrometric methods.

Though, there are various methods as we have seen for the sucrose measurement so far but all the methods have some shortcoming, particularly they all are time consuming. Over the past few decades, extensive researches have been done for Raman spectroscopy all over the world. The researches have been made to correlate the Raman spectra of biological materials with their structural features. Despite certain difficulties and experimental limitations great success has been attained for Raman spectroscopy. Nowadays, laser-Raman spectroscopy has become a powerful tool in the structural study of biologically important compounds. However most such studies were on the proteins and nucleic acids and only a few on carbohydrates. Among the saccharides, D-glucose has been the most extensively studied compound [25].

## 1.5 The Raman Spectroscopy

The phenomenon of inelastic scattering of light by matter was first observed experimentally by C.V. Raman, an Indian physics professor, and his colleague K.S. Krishnan in 1928 (Raman and Krishnan 1928). In 1930, he won the Nobel Prize in physics for his work on the scattering of light and for the discovery of the effect named after him.

### 1.5.1 Conventional Raman Effect

When a sample is irradiated with an intense monochromatic light source (usually a laser), most of the radiation is scattered by the sample at the same wavelength as that of the incoming laser radiation in a process known as Rayleigh scattering. However, a small proportion of the incoming light, approximately one photon out of a million is scattered at a wavelength that is shifted from the original laser wavelength, this phenomena is known as Raman effect.

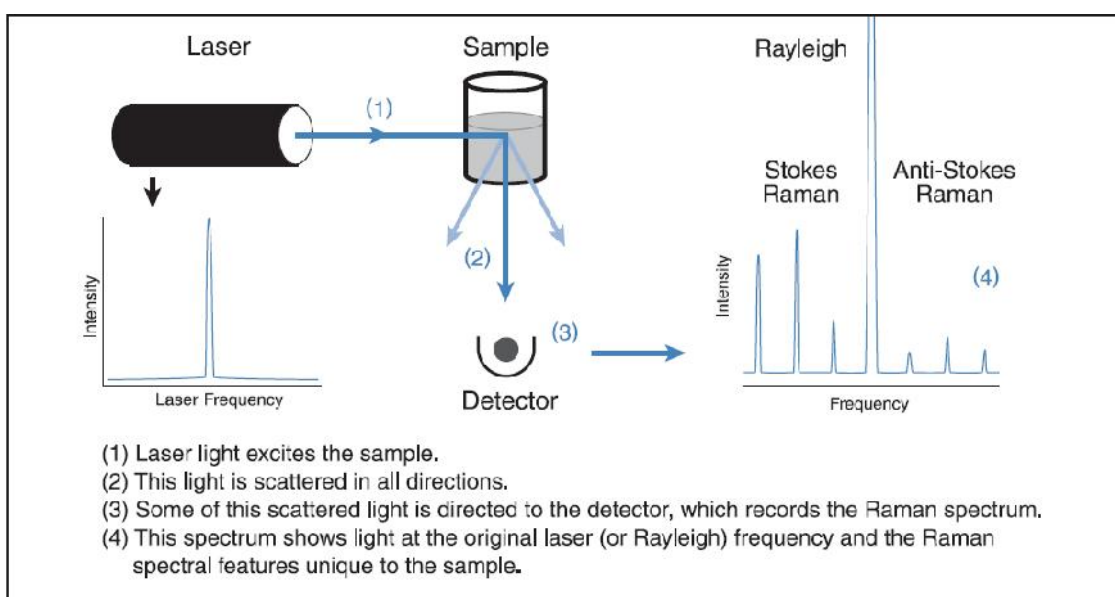


Figure 1.7: Overview of conventional Raman effect

As illustrated in the simplified energy level diagram (Fig. 1.8), a molecule at rest resides in the ground vibrational and electronic states. The electric field of the laser beam raises the energy of the system for an instant by inducing a polarization in the chemical species. The polarized condition is not a true energy state and is referred to as a “virtual state”. Relaxation from the virtual state occurs almost instantaneously and is predominantly to the initial ground state. This process results in Rayleigh scatter, which is scattered light of

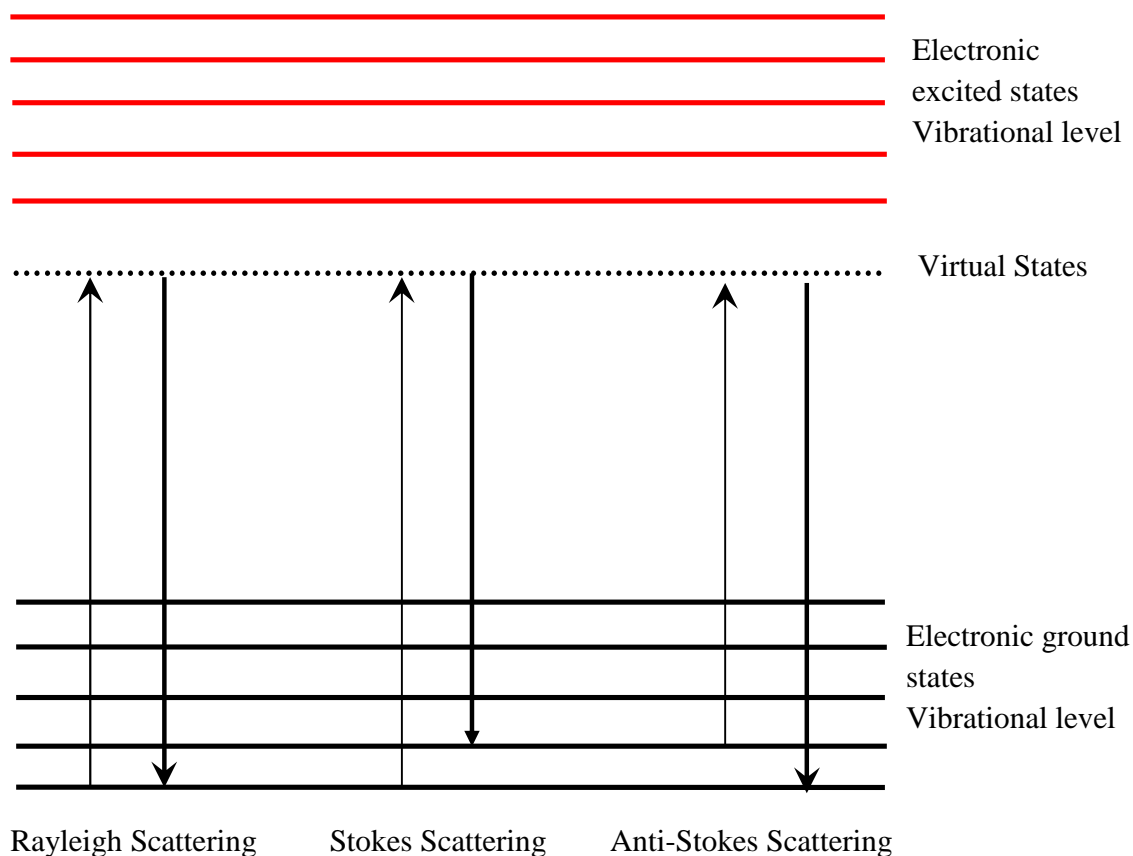


Figure 1.8: Energy level diagram

the same wavelength as the excitation laser. Relaxation to the first excited vibrational level results in a Stokes-Raman shift. Stokes-Raman shift scattered light is of lower energy (longer wavelength) than that of the laser light. In addition, most systems have at least a small population of molecules that are initially in an excited vibrational state. When the Raman process initiates from the excited vibrational level, relaxation to the ground state is possible, producing scatter of higher energy (shorter wavelength) than that of the laser light. This type of scatter is called anti-Stokes Raman scatter.

The vibrational states probed by Raman spectroscopy are similar to those involved in infrared spectroscopy. However, the two vibrational spectroscopy techniques are complementary, in that vibrations that are strong in an infrared spectrum (those involving strong dipole moments) are typically weak in a Raman spectrum. Likewise, non-polar functional group vibrations that give very strong Raman bands usually result in weak infrared signals.

Raman spectroscopy provides key information about the structure of molecules. The position and intensity of features in the spectrum reflect the molecular structure and can be used to determine the chemical identity of the sample. Spectra may also show

subtle changes depending on the crystalline form. With the extensive spectral libraries that are now available, it is very straightforward to identify compounds by spectral library searching. Raman spectrometers are generally based on one of two technologies: **dispersive Raman** and **Fourier transform Raman**.

### **1.5.2 Dispersive Raman Spectroscopy**

Dispersive Raman usually employs visible laser radiation. Typical laser wavelengths are 780 nm, 633 nm, 532 nm, and 473 nm; others are also used. The intensity of the Raman spectra is proportional to  $1/\lambda^4$ , so short excitation laser wavelengths deliver a much stronger Raman signal. Although this would suggest that all Raman should be collected using the shortest wavelength lasers, but fluorescence is also much more likely to occur under these conditions, and therefore, it is very difficult to obtain reasonably good spectra, especially for the naturally occurring sucrose and sugars in food products. As these materials are not pure, they frequently suffered from the fluorescence when excited with visible laser light. Thus, Raman spectra, superimposed on a strong fluorescent background are practically useless for any analytical purpose. Moreover, such sensitive materials as plants may decompose (dehydrate or burn) under the strong laser radiation. Hence, though dispersive Raman spectroscopy has several advantages over other analytical methods but it cannot be used in some cases successfully.

However, there is a great anticipation connected with the application of Fourier transform (FT) Raman spectroscopy, which usually utilizes the NIR laser light which is the remedy for the problems as said in the application of dispersive Raman spectroscopy.

### **1.5.3 FT-Raman Spectroscopy**

FT-Raman spectrometer employs a laser in the near infrared usually a 1064 nm rather than visible laser radiation as employed in dispersive Raman spectroscopy. It has been already proved that the use of near-infrared Nd/YAG laser at 1064 nm as an excitation source drastically reduces the fluorescence that hampers conventional Raman spectra [39]. Moreover, the measurements are practically non-destructive and no sample preparation is required prior to FT-Raman spectroscopy. However because of the  $1/\lambda^4$  relationship between Raman scattering intensity and wavelength, the Raman signal becomes very weak. In addition, silicon CCD detectors cannot be used in this region of the spectrum. FT-Raman uses sensitive, single-element, near-infrared detectors such as indium gallium arsenide (InGaAs) or liquid nitrogen-cooled germanium (Ge) detectors such as indium gallium arsenide (InGaAs) or liquid nitrogen-cooled germanium (Ge) detectors. An interferometer converts the Raman signal into an interferogram, permitting

the detector to collect the entire Raman spectrum simultaneously. Since at low signal levels the spectral noise is predominantly detector dark noise and is independent of the intensity of the Raman signal, delivering the entire spectrum at once onto the detector greatly improves the signal to- noise ratio. Application of the Fourier transform algorithm to the interferogram converts the results into a conventional Raman spectrum.

Some other varieties of the Raman spectroscopic techniques have been also developed in the art as being either useful or potentially useful in many applications. For example, there is disclosed a non-invasive blood glucose measurement system and method using stimulated Raman spectroscopy [40]. The system and method make use of two monochromatic laser beams, a pump laser beam and a probe laser beam. The output power of the pump laser beam is amplitude modulated, combined with the probe laser beam and directed into the ocular aqueous humor of a living being. The introduction of the laser beams into the ocular aqueous humor induces scattered Raman radiation, which causes a portion of the energy at the pump frequency to shift over to the probe frequency. The pump and probe laser beams are then detected as they exit the ocular aqueous humor. The probe laser beam is filtered, converted into an electrical signal and then amplified. Thereafter, it is compared to the modulation signal to generate an electrical signal representative of the concentration of **D-glucose** in the ocular aqueous humor.

Although, there are a variety of techniques in which Raman spectroscopy can be employed. For example, spontaneous Raman spectroscopy, coherent anti-stokes Raman spectroscopy and pulse-pumped stimulated Raman spectroscopy but all these techniques have some disadvantages. For example, there is a problem of fluorescence associated with spontaneous Raman spectroscopy, coherent anti-stokes Raman spectroscopy and pulse-pumped stimulated Raman spectroscopy typically require a long exposure time (several minutes ) and high power laser pump that exceeds the safety limitations by laser illumination for biological material tested. As can readily be appreciated, requirements such as these substantially limit the practical applicability of these techniques in many fields. Therefore, now we are going to discuss a novel method known as “Low Power Continuous Wave (CW) Excitation Raman Spectroscopy” which will eliminate the problems as said above.

## 1.5.4 Low Power Continuous Wave (CW) Excitation Raman Spectroscopy

To overcome the difficulties as said above in Raman spectroscopic measurement for biological materials, a new method were discovered titled as “Method and system for examining biological materials using low power continuous wave (CW) excitation Raman spectroscopy” [41]. In accordance with this invention, the system and the method employing a low power continuous wave (CW) pump laser beam and a low power CW Stokes (or anti-Stokes) probe laser beam. The pump beam and the probe beam simultaneously irradiate the biological material and traverse the biological material in collinearity. The pump beam whose wavelength is varied, resulting in changed in pump beam frequency is used to induce Raman scattering from the biological material. The intensity of the probe beam is fixed by keeping the probe wavelength constant (i.e., resulting frequency is constant) is monitored as when leaves the biological material. When the difference between the pump ( $\Omega$ ) and probe ( $\omega$ ) excitation frequencies is equal to a Raman vibrational mode frequency ( $\nu$ ) of the biological material, the weak probe signal becomes amplified by one or more orders of magnitude (typically up to about  $10^4 - 10^6$ ) due to the Raman scattering from the pump beam. In this manner, by monitoring the intensity of the probe beam emitted from the biological material as the pump beam is varied in frequency (i.e., by tuning the wavelength of the pump beam), one can obtain an excitation Raman spectra for the biological material examined.

It is noted that, this method may be applied to in the in vivo and/or in vitro diagnosis of diabetes, heart disease, hepatitis, cancers and other diseases by measuring the characteristic excitation Raman lines of blood **glucose**, cholesterol, serum glutamic oxalacetic tansaminase (SGOT)/serum glutamic pyruvic transaminase (SGPT), tissues and other corresponding Raman-active body constituents, respectively. It may also be used to diagnose diseases associated with the concentration active constituents in urine, lymph and saliva. It may be used to identify cancer in the breast, cervix, uterus, ovaries and the like by measuring the fingerprint excitation Raman spectra of these tissues. It may also be used to reveal the growing of tumours or cancers by measuring the levels of nitric oxide in tissue.

One of the advantage of this method is that the experiment can be performed in a very short detecting time (i.e., on the order of several seconds as opposed to several minutes) and the major advantage is that the pump and the probe beams can be operated at a power of up to four orders of magnitudes less than that typically used in the pulsed coherent Raman spectroscopic techniques.

When only the pump laser light is irradiated to the any biological material, a weak spontaneous Raman signal is scattered by the biological material in response to the pump laser light. This is illustrated in the Fig. 1.9.

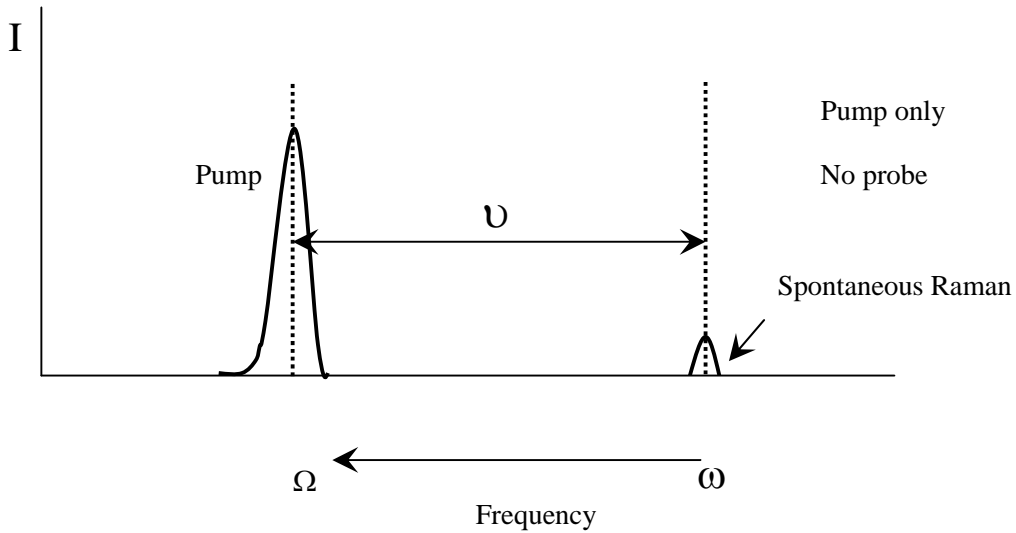


Figure 1.9: Pump laser signal and scattered spontaneous Raman signal

When only the probe laser light is irradiated to any biological material, the result is a weak spontaneous Raman signal not even being shown (Fig. 1.10). This spontaneous Raman signal is very weak in contrast with the spontaneous Raman signal emitted by the biological material, when only the pump laser light is irradiated to the biological material (see Fig. 1.9).

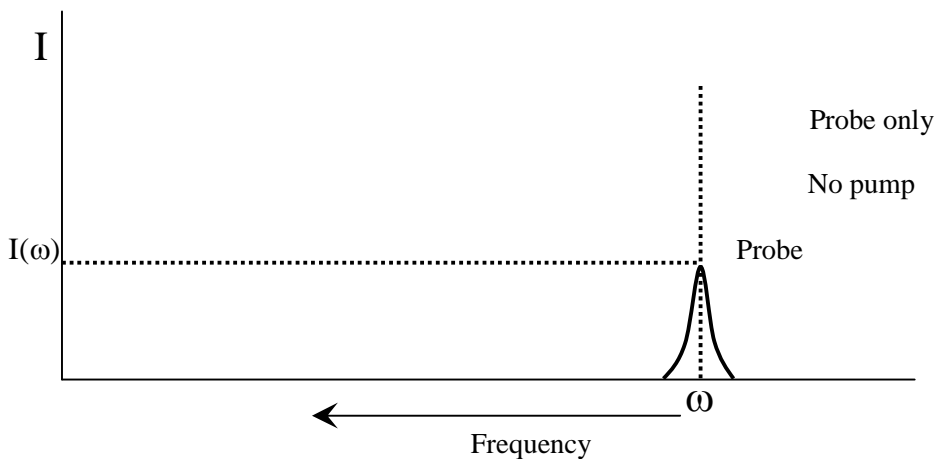


Figure 1.10: Irradiated probe signal

When the pump laser and probe laser light are irradiated simultaneously to the any biological material and in addition when the pump laser light frequency ( $\Omega$ ) is tuned in





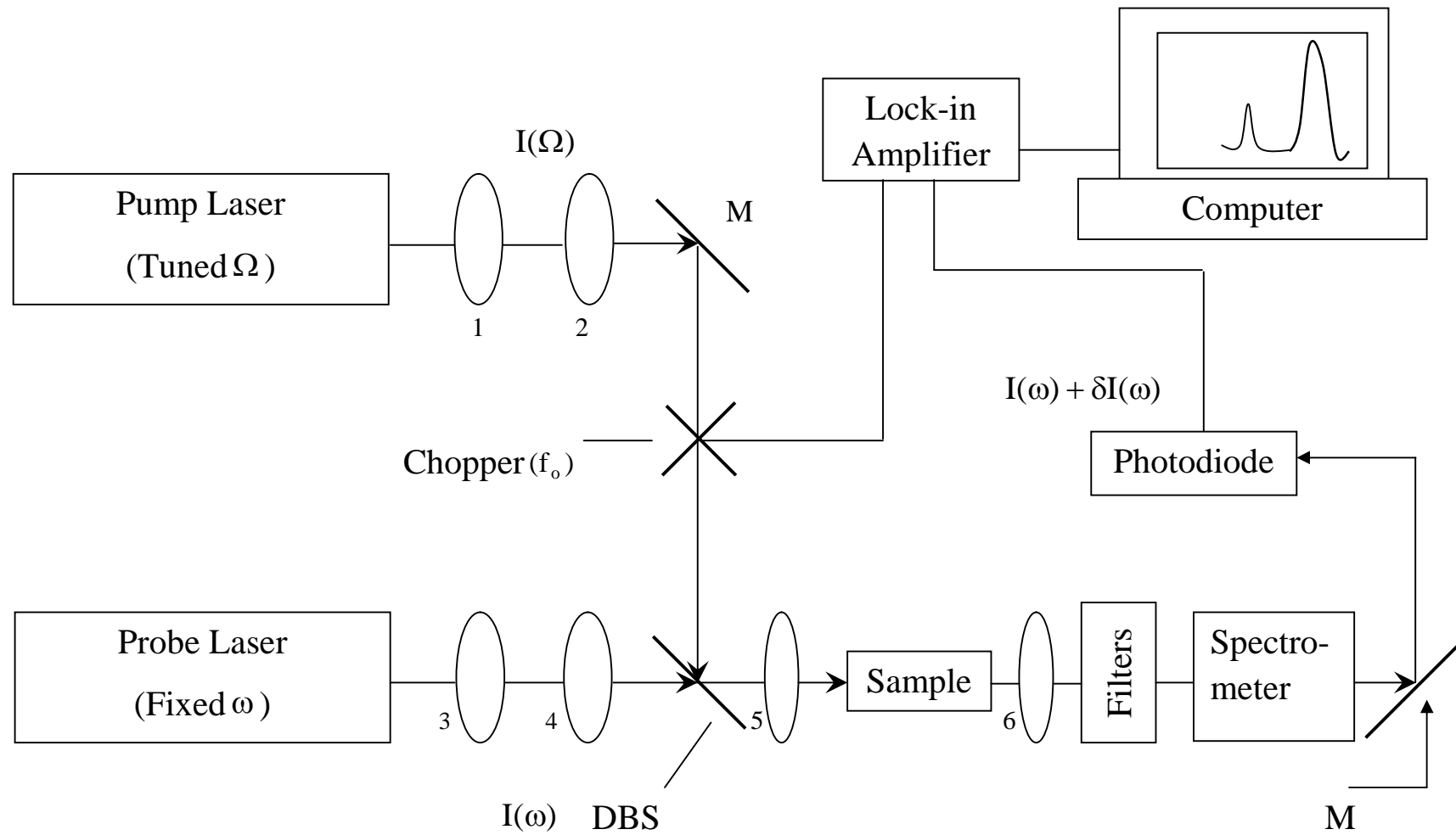


Figure 1.12: Schematic of the low-power CW Raman spectroscopy

signal  $\delta I(\omega)$  at the probe wavelength reflects the Raman gain produced by the modulated beam. The filtered light is sensed by the photodiode or a photomultiplier. The probe signal sensed by the photodiode is amplified and demodulated by the lock-in amplifier and then the demodulated signal is processed by the computer. The excitation Raman spectra is plotted on the monitor.

### **1.5.6 Measurement of Sucrose by Low Power CW Raman Spectroscopy**

One of the main objective of the second part of the thesis is to measure the quantity of sucrose content by low power continuous wave Raman spectroscopy, i.e., we are interested only in quantitative measurement not qualitative. As we have already seen that any biological material can be investigated qualitatively and quantitatively by low power continuous wave Raman spectroscopy method [41]. Therefore, the set-up for the measurement of sucrose content we are going to propose is a little modification of the actual set-up as illustrated in the Fig. 1.12. It is interesting to note that the measurement method is the same but with a little modification in the measurement set-up we can measure the sucrose quantitatively.

In the proposed set-up we are going to employed two fixed laser light instead of one tuned and one fixed laser light [41]. In this set-up we are not going to use the mechanical chopper for the modulation of the pump laser light because it is bulky. Here we are going to modulate the pump beam electronically and to perform the modulation process electronically we are using a square wave as an excitation to the pump laser.

Since we are specifically interested in the quantitative measurement of the sucrose and therefore, we don't require the whole spectrum to analyze the sucrose qualitatively. For that reason, we haven't used spectrometer in our proposed method. In this work, we are interested only in the Raman spectra of sucrose where the intensity of the amplified signal at the probe wavelength attains its peak value and It has already been shown that intensity of the Raman spectra of sucrose solution attain its peak value corresponding to the Raman shift  $836\text{ cm}^{-1}$ , when the solutions having the ratio 24 & 66% (w/w) concentration [42].

Referring to the Fig.1.13, and table 1.3, it can be seen that the relative intensity of the Raman spectra is maximum at the Raman shift of  $836\text{ cm}^{-1}$ . In our proposed method we are going to use one laser diode of wavelength 785 nm and as we already know the Raman shift corresponding to the maximum Raman intensity [42]. Therefore the wavelength of the probe laser beam can be easily determined so that the difference between the pump laser beam frequency ( $\Omega$ ) and the probe laser beam frequency ( $\omega$ ) irradiated onto the biological material sample equals to the Raman vibrational mode

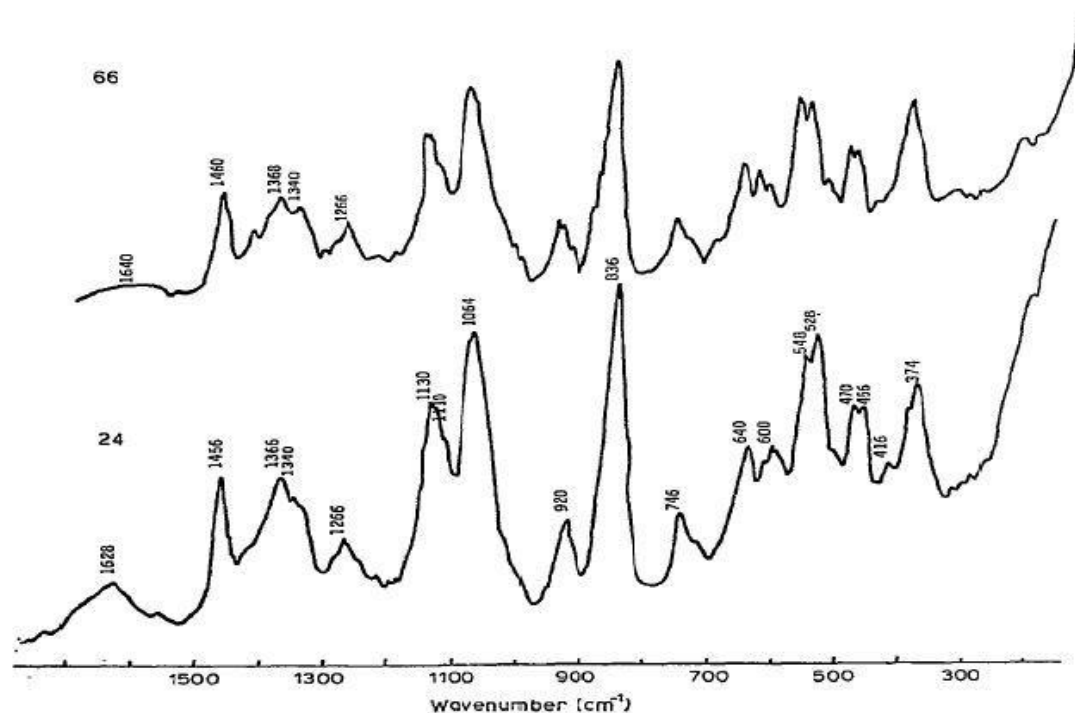


Figure 1.13: Raman spectra of the sucrose solution at 24 & 66% (w/w) concentration

$\nu$ ( $\text{cm}^{-1}$ )	$I$	$\rho$	Assignments
1628	16.4	0.56	$\delta$ (HOH)
1456	33.6	0.93	$\delta$ (CH <sub>2</sub> )
1366	45.7	0.67	w (CH <sub>2</sub> )
1340	37.8	0.72	r (CH <sub>2</sub> )
1266	25	0.71	$\tau$ (CH <sub>2</sub> )
1130	68	0.53	$\delta$ (COH)
1110	60	0.20	$\nu$ (C-O) <i>endo</i>
1064	89	0.31	$\nu$ (C-O) <i>exo</i>
920	25	0.34	$\delta$ (C-H)
836	100 <sup>b</sup>	0.10	$\nu$ (C-C)
746	21	0.38	$\delta$ (CCO) <i>endo</i> (Fru)
640	35.7	0.24	$\delta$ (CCO) <i>exo</i> (Fru)
600	31.4	0.45	$\delta$ (OCO <sub>1</sub> )
548	60.7	0.25	$\delta$ (CCO) <i>endo</i> (Glc)
528	69	0.17	$\delta$ (CCO) <i>exo</i> (Glc)
470	38	0.10	$\delta$ (CCC) (Fru)
456	36.4	0.23	$\delta$ (CCC) (Glc)
416	17.8	0.84	$\delta$ (O-H-O)
374	40	0.25	$\delta$ (COC)

<sup>a</sup>Key:  $I$  = relative intensity,  $\rho$  = depolarization ratio, *endo* = endocyclic, *exo* = exocyclic, Fru = D-fructosyl moiety, Glc = D-glucosyl moiety,  $\delta$  = bending mode, w = wagging, r = rocking,  $\tau$  = twisting, and  $\nu$  = stretching mode. <sup>b</sup>Reference standard.

Table 1.3: assignment of the frequencies observed in the spectra of the sucrose in aqueous solutions

frequency ( $\nu$ ) of the sample and by applying the method as said, the required wavelength of the probe laser beam comes around 840 nm. Thus, in our work we are going to use two low power laser beams of wavelength 785 nm and 840 nm. Wavelength of 840 nm laser beam will serve as probe beam and wavelength of 785 nm laser diode will serve as pump laser beam. The proposed set-up is illustrated in Fig. 1.14.

### **1.5.7 Working Principle of Proposed Low Power Continuous Wave (CW) Raman Spectroscopy**

The proposed schematic of low power Low Power Continuous Wave (CW) Raman Spectroscopy is shown in the Fig. 1.14. The system includes two laser beams, in which one is usually called pump laser and other is called the probe laser. In this system pump laser beam is modulated electronically instead of using mechanical chopper as used in actual set-up (Fig.1.12). The pump laser beam of 785 nm and probe laser beam of 840 nm passes through the lenses namely 1-4, mirrors M and a dichroic beam splitter DBS. The purpose of the dichroic beam-splitter is to combine the pump and probe beams and to adjust them for collinearity. The combined pump and the probe laser beams are then focused by the lens 5 onto the sample. Light scattered by the sample is then collected by the lens 6 and then filtered by the selective filter. The selective filter then collects all the scattered light which is at wavelength 840 nm and rejects especially 785 nm wavelength and lights which are not at probe wavelength. . The modulated signal  $\delta I(\omega)$  at the probe wavelength reflects the Raman gain produced by the modulated beam. The filtered light is sensed by the photodiode or a photomultiplier. The probe signal sensed by the photodiode is amplified and demodulated by the lock-in amplifier. In our work we are performing the operation of lock-in amplifier through the software Labview 8.5. Thereafter, the demodulated signal is processed by the computer and then the excitation Raman spectra are plotted on the monitor.

It can be noted that this method is only applicable to the quantitative measurements and the Raman shift of the biological sample must be known in advance so that the wavelength of the probe beam can be determined by the method said. Since, we already know the Raman shift corresponding to the maximum intensity for the sucrose measurement. Therefore, the proposed method can easily applied for the sucrose content measurement by using one 785 nm laser diode and one 840 nm laser diode.

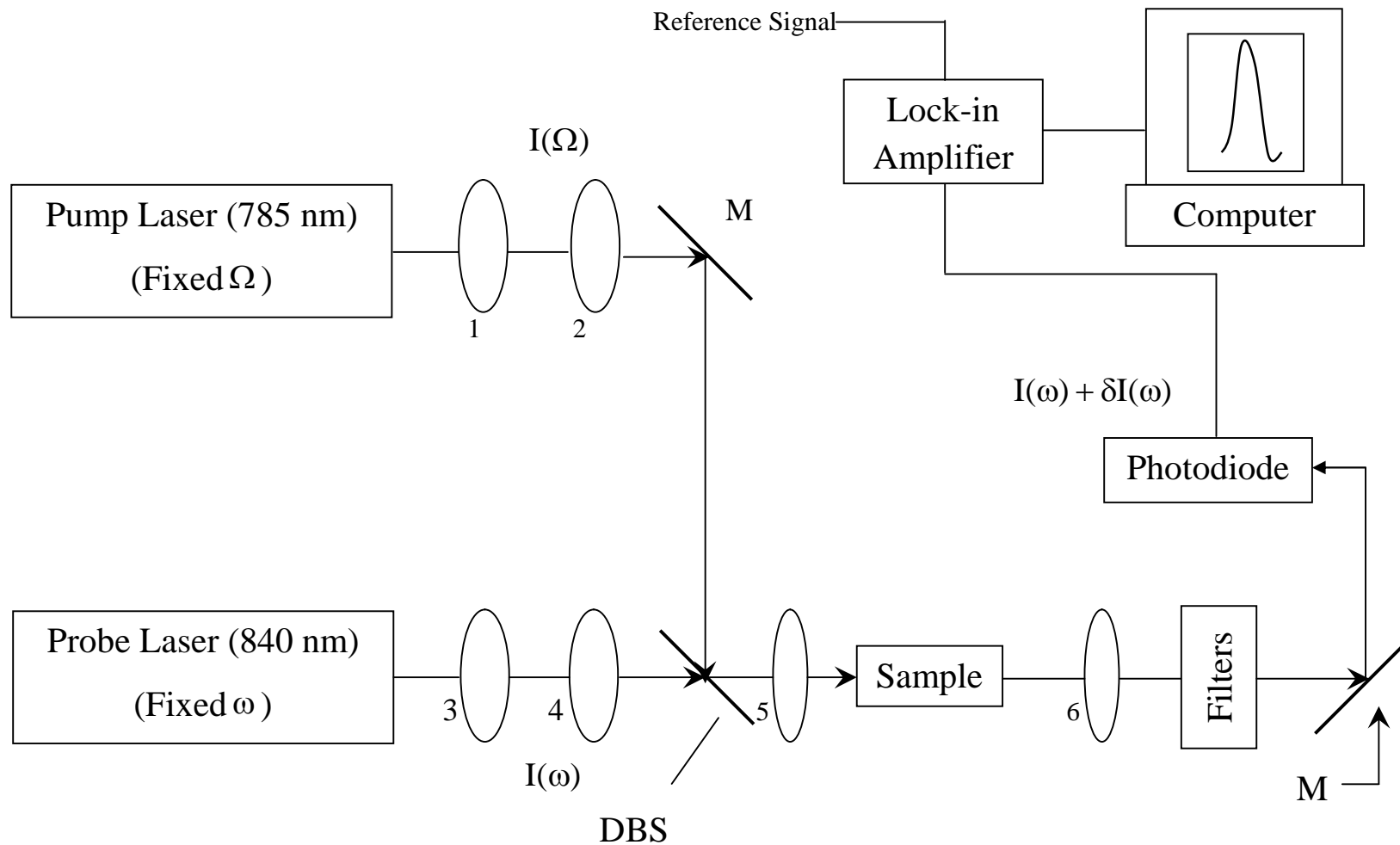


Figure 1.14: Schematic of the proposed low-power CW Raman spectroscopy

## 1.5.8 Objectives and Organization of this Thesis

This thesis has two main parts: the first part is about sap flow measurements and second part is about measurement of sucrose content by Raman spectroscopy.

**In the first part**, the objective is to measure and analyze the sap flow rate using the sap flow meter (SGA5) in stem of the virtual plant. SGA5 is a Sap flow sensor usually called micro flow gages manufactured by Dynamax Inc. and Virtual Plant Model (VPM) is an experimental set up in which water flows through the PVC pipe of diameter 5 mm and flow rate can be precisely control by syringe infusion pump (LPM-50DN) and by installing the sap flow meter (SGA5) in the stem of the Virtual plant model, we can measure and then analyze the flow rate of the sap.

So, the biggest challenge is to design the Virtual plant model in which water flowing through the PVC pipe should exactly match to the sap flow mechanism. Therefore, in order to do so, we made sever configuration of the virtual plant model so that we can simulate the stem of the virtual plant model exactly to the stem of any real plant.

To get the stable and satisfactory results we have taken several readings and we have also modified the design several times of the virtual plant model. We have made total four different design of the virtual plant model, in which two of them worked satisfactory. Two of the designed virtual plant model worked satisfactory but unfortunately that was failed to measure the higher flow rate. But those designs have given the satisfactory results for the medium range flow rate (6 ml/h to 10 ml/h).

The other objectives are to be familiar with the sap flow meter, studying about its working equations, electrical and mechanical specifications of the sensor, its features, benefits, and its applications.

In this chapter, initially we have seen that how the sap flow measurements methods have been evolved since Huber's [1] work then, the SHB technique first proposed by Vieweg and Ziegler [8] and later by Daum [9], and Steady-state assumption by Sakuratani [12, 13] and the subsequent development by Baker and Van Bavel [14] and steinberg [15]. Thereafter we have seen the designed and measurements method developed by Sakuratani [12, 13] and Baker and Van Bavel [14] in great detail. We have also talked about the dynamic response, applications of the sap flow gage (especially monitored by Dynagage Inc. [23]) and systems for monitoring sap flow (Flow32 sap flow system [23]).

**In the second part**, the objective is to measure sucrose content by the method "Low Power continuous wave (CW) Raman Spectroscopy" [41]. This method has been discovered by the inventors Robert R. Alfano, Bronx; Wubao Wang, Flushing. Therefore, in this chapter we have talked about different methods for the measurement of sucrose,

conventional Raman effect, dispersive Raman spectroscopy, FT- Raman spectroscopy, and the limitations of these techniques and to overcome these limitations, we have seen a novel method “low power continuous wave (CW) excitation Raman spectroscopy” [41] and in the end of this chapter, we have given a proposed method for the measurement of the sucrose content.

In **chapter 2**, we first talk about the sensor and the other components used for the measurement of the sap flow rate. Then we will study about the working principle of sensor, construction and its specifications. Thereafter we will see the detailed design of the virtual plant model. We will also talk about the instrument and the components which have been used to design the virtual plant. Then we will see the necessary hardware circuit design to amplify the signals coming from the sensor. Prior to the measurement we will see the complete experimental set up used for the flow measurement of the sap.

In **chapter 3**, we begin with the experiment, results, and the problems faced during the measurement. We will also see the different design of the virtual plant to continuously improve the results and the accuracy of the flow rate. Based on the available data we will first determine the practical flow rate and then we will compare with the actual flow rate. Observing the difference between the practical sap flow rate and the actual flow rate we will discuss about the problems in the virtual plant model and its remedy to improve the results further.

Thereafter we will see the conclusions and in the end we will talk about the future scope of this work.

## References

- [1] Huber, B. 1932. Beobachtung and Messung pflanzlicher Saftstrome. Ber. Deutsch. Bot. Ges. 50:89-109
- [2] Bloodworth, M.E., J.B. Page, and W.R. Cowley, 1955. A thermoelectric method for determining the rate of water movement in plants. Proc. Soil Sci. Soc. Amer. 19:411-414
- [3] Closs, R.L. 1958. The heat pulse method for measuring rate of sap flow in plant stem. New Zealand J. Sci. 1:281-288
- [4] Swanson, R.H. 1972. Water transpired by trees as indicated by heat pulse velocity. Agr. Met. 10:277-281
- [5] Lassoie, J.P., D.R.M. Scott, and L.J. Fritschen. 1977. Transpiration studies in Douglas fir using heat pulse technique. For. Sci. 23:377-390
- [6] Miller, D.R., C.A. Vavrina, and T.W. Christensen. 1980. Measurement of sap flow and transpiration in ring-porous oaks using heat pulse velocity technique. For. Sci. 26:485-495
- [7] Cohen, Y., M. Fuchs, and G.C. Green. 1981. Improvement of the heat pulse method for determining sap flow in trees. Plant Cell Env. 4:391-397
- [8] Vieweg, G.H. and H. Ziegler. 1960. Thermoelektrische Registrierung der Geschwindigkeit des Transpirationsstromes. Ber. Deutsche Bot. Ges. 73:221-226
- [9] Daum, C.R. 1967. A method for determining water transport in trees, Ecology 48:425-431
- [10] Ermák J, Deml J, Penka M 1973 A new method of sap flow rate determination in trees. Biol Plant 15:171-178
- [11] Ermák J, Jeník J, Kucera J, Zidek V 1984 Xylem water flow in a crack willow tree (*Salix fragilis* L.) in relation to diurnal changes of environment. Oecologia (Berlin) 64: 145-151
- [12] Sakuratani, T. (1981) A heat balance for measuring water flux in the stem of intact plants, Journal of Agricultural Meteorology, 37, 9-17
- [13] Sakuranatni, T. (1984) Improvement of the probe for measuring water flow rate in intact plants with the stem heat balance method. Journal of Agricultural Meteorology, 40, 273-277
- [14] Baker, J.M. and C.H.M. van Bavel. 1987. Measurement of mass flow of water in stems of herbaceous plants. Plant, Cell, and Environment 10: 777-782.
- [15] Steinberg, S. 1988. Dynamax Trunk-Flow Gauge Test, Technical Application Report 2. Insulation and Time of Attachment Test. Dynamax Inc.
- [16] Hinckley, T.M., Brooks, J.R., Cermak, J., Ceulemans, R., Kucera, J., Meinzer, F.C. and Roberts, D.A. 1994, Water flux in a hybrid poplar stand. Tree Physiology 14, 1005-1018



- [17] Groot A, King KM. 1992. Measurement of sap flow by the heat balance method: numerical analysis and application to coniferous seedlings. *Agricultural and Forest Meteorology* 59, 289-308
- [18] Baker, J.M., and J.L. Nieber. 1989. An analysis of the steady-state heat balance method for measuring sap flow in plants. *Agric. For. Meteorol.*, 48:93-109.
- [19] Dugas, W.A., 1990. Comparative measurement of stem flow and transpiration in cotton. *Theor. Appl. Climatol.*, 42:215-221
- [20] Shackel KA, Johnson RS, Medawar CK, Phene CJ. 1992. Substantial errors in estimates of sap flow using the heat balance technique on woody stems under field conditions. *Journal of the American Society for Horticultural Science*
- [21] H.S. Carslaw and J.C. Jaeger, *conduction of heat in solids* (Clarendon, Oxford, 1959), pp 425-426
- [22] Ku era J, ermák J, Penka M 1977 Improved thermal method of continual recording the transpiration flow rate dynamics. *Biol Plant* 19:413-420.
- [23] Dynamax Inc. 1990. Dynagage Users manual. Houston, TX
- [24] <https://apps.fas.usda.gov/psdonline/circulars/sugar.pdf>
- [25] M. Mathlouthi, C. Luu, A.M. Meffroy-Biget and D.V. Luu, Laser-Raman study of solute-solvent interactions in aqueous solutions of D-fructose, D-glucose, and sucrose, *Carbohydr. Res.* 81 (1980), 203–212
- [26] H. Basciano, L. Federico and K. Adeli, Fructose, insulin resistance, and metabolic dyslipidemia, *Nutr. Metab.* 2 (2005), 1–14
- [27] W.C. Willett, Dietary fat plays a major role in obesity, *Obes. Rev.* 3 (2002), 59–68.
- [28] T.S. Cunha, V. Faraha, J. Paulini, M. Pazzine, K.M. Elased, F.K. Marcondes, M.C. Irigoyen, K. De Angelis, L.D. Mirkin and M. Morris, Relationship between renal and cardiovascular changes in a murine model of glucose intolerance, *Regul. Pept.* 139 (2007), 1–4
- [29] M. Fisberg, C.R.S. Bandeira, E.A. Bonilha, G. Halpern and M.D. Hirschbruch, Hábitos alimentares na adolescência, *Pediatr. Mod.* 36 (2000), 724–734
- [30] C.R.M. Frazier, P. Mason, X. Zhuang and J.A. Beeler, Sucrose exposure in early life alters adult motivation and weight gain, *PLoS ONE* 3 (2008), 3221
- [31] Eggins B (2002) 'Chemical sensors and biosensors'
- [32] Soldakin O, Peshkova V, Dzyadevych S (2008) Novel sucrose three-enzyme conductimetric biosensor. *Materials Science and Engineering* 28, 959–964
- [33] Guemas Y, Boujtita M, Murr Ne (2000) Biosensor for determination of glucose and sucrose in fruit juices by flow injection analysis. *Applied Biochemistry and Biotechnology* 89, 171–181.

- [34] Gouda MD, Kumar MA, Thakur MS, Karanth NG (2002) Enhancement of operational stability of an enzyme biosensor for glucose and sucrose using protein based stabilising agents. *Biosensors and Bioelectronics* 17, 503–507
- [35] Kennedy J, Pimentel M, Melo E, Lime-Filho J (2007) Sucrose biosensor as an alternative tool for sugarcane field samples. *Journal of the Science of Food and Agriculture* 87, 2266–2271.
- [36] Surareungchai W, Worasing S, Sritongkum P (1999). Dual electrode signal subtracted biosensor for simultaneous flow injection determination of sucrose and glucose. *Analytica Chimica Acta* 380, 7–15
- [37] R.N. Silva, V.N. Monteiro, J.X. Alcanfor, E.M. Assis and E.R. Asquieri, Comparação de métodos para a determinação de açúcares redutores e totais em mel, *Ciência Tecnol. Alime.* 23 (2003), 337–341
- [38] N. Ghosh, Y. Verma, S.K. Majumder and P.K. Gupta, A fluorescence spectroscopic study of honey and cane sugar syrup, *Food Sci. Technol. Res.* 11 (2005), 59–62
- [39] Ellis,G.,Hendra,P.J.,Hodges,C.M.Jawhari, T., Jones, C.H.,Le Barazer, P.,Passingham, C., Royaud, I.A.M., Sanchez-Blasquez,A.&Warnes,G.M.(1989). Routine analytical Fouries transform Raman spectroscopy. *The Analyst*, 114, 1061-1066
- [40] “Non-invasive blood glucose measurement system and method using stimulated raman spectroscopy” US. Pat. No. 5,243,983
- [41] “Method and system for examining biological materials using low power continuous wave (CW) excitation Raman spectroscopy” US. Pat. No. 6,151,522
- [42] M. Mathlouthi and Dang Vinh Luu “Laser-Raman spectra of D-glucose and sucrose in aqueous solution”

\*\*\*\*\*

## Chapter 2

### Virtual Plant Model

#### 2.1 Theory of the Sap Flow Meter

Sap flow meters produced by Dynamax Inc. are the instruments used for the measurement of sap-flow in the herbaceous plants and trees. A stem heat balance method derived from a constant heat source monitors sap flow in plants from 2 mm (0.1") to 150mm (6") in diameter. It is based on the electronic sensing method with three output signal per sensor. The sensors sense millwatt power transfers from a heater element to the ambient, to the stem of the plant, and into the sap flow. Sap decreases the temperature generated by the heater in varying amounts corresponding to the flow rate. Two readings from the thermocouples which measure the temperature difference below and above the heater and simultaneously measure the stem heat transfer. A third reading from the sensor measures the radial heat flux, the heat lost to the ambient, from the thermopile. The stem heat balance (SHB method also requires monitoring the voltage continuously to the heater so that the constant energy input is known with precision. Thus, we require a total of four data to monitor all the signals pertaining to the sap flow computations.

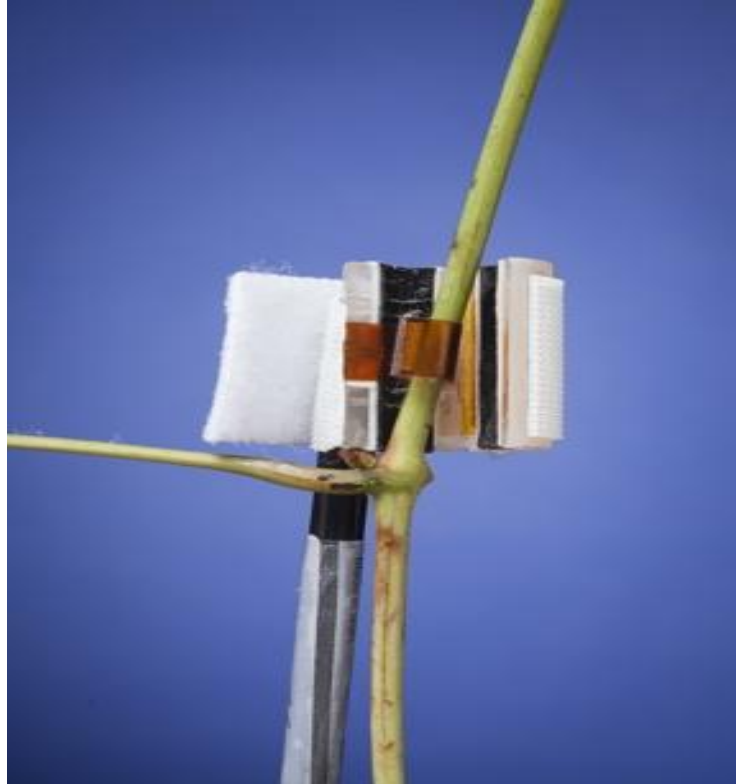


Figure 2.1: Schematic of Dynagage sap sensor

## 2.2 Sap Flow Meter Specifications and its Body Construction

Sap flow meters have a soft foam collar that surrounds the electronics. The unit is installed on a stem having an axial length of at least the gage height, which is cleared of branches and smoothed. A weather shield is installed for outdoor applications and radiation shielding. The specification for the gage diameter is the determining factor for selection of a gage, which fits properly. Choosing a gage that is the typical size or, close to the minimum size will provide ample room for plant growth. The sensor can also be moved higher on the stem to fit a smaller diameter or lower to fit a larger diameter. An insulation wedge can be obtained to fill the gap when expanding the gage to the maximum diameter limit. Above the maximum diameter, the heater strip will not completely encircle the stem or trunk, causing insufficient and uneven heating.

Note: In this present work we used Micro flow gage (**SGA5-ws**)

Table 2.1: Mechanical Specifications

Model No.	Gage Height (mm)	Shield Height (mm)	Stem Diameter (mm)			TC Gap dX (mm)	NO. Pairs	Input Voltage (Volt)	Input Power (Watt)
			Min.	Typ.	Max.				
<b>Micro Flow Gages</b>									
SGA5-ws	35	70	5	5.0	7.0	3.0	2	4.0	.08

## 2.3 Electrical Specifications

The recommended operating conditions vary by the stem diameter and the heat requirement of the water to obtain easily measurable results. For initial gage start-up, low-level radiation in various laboratory conditions, or winter (low level) flow rates, the minimum input to the heater must be used. To achieve the best results over medium flow rates the typical voltage is recommended to supply heater power.

Table 2.2: Heater input voltage

Heater input voltage D.C. Measured at device terminals D (+), E (-)				
Part Number	Minimum	Typical	Maximum	Unit
SGA5-ws	3.5	4.0	4.5	Volt

Table 2.3: Heater input power

Heater input Power Recommended for each; $P_{in} = V^2/R$				
Part Number	Minimum	Typical	Maximum	Unit
SGA5-ws	.05	.08	.10	Watt

Table 2.4: Heater impedances

Heater impedances A 10% variation from unit to unit is normal.				
Part Number	Minimum	Typical	Maximum	Unit
SGA5-ws	170	190	200	Ohm

## 2.4 Sap Sensor Construction

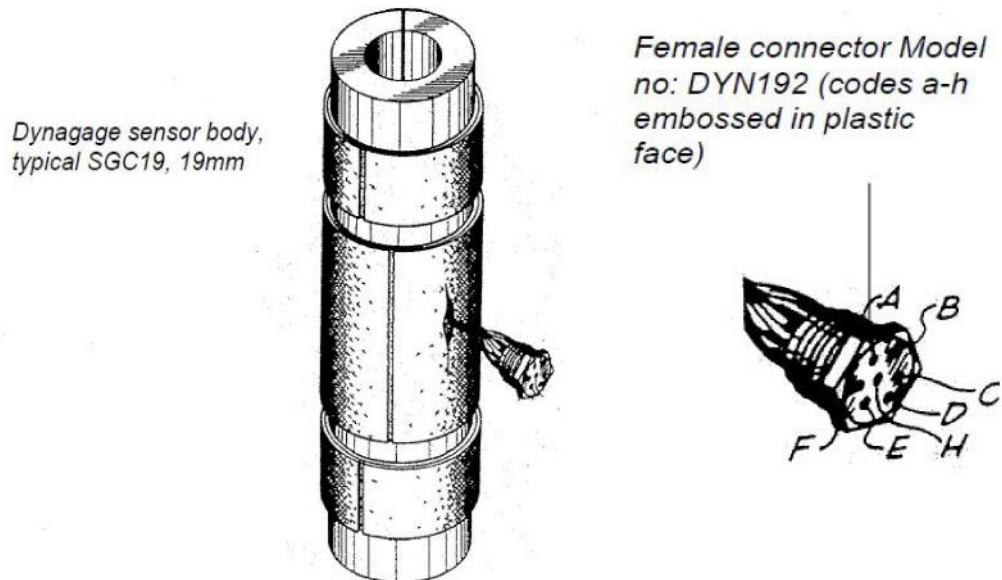


Figure 2.2: Construction of Dynagage sensor and female connector Model

## 2.5 Design of the Virtual Plant Model.

The virtual plant is basically an experimental set up in which water flows through the pipe and flow rate can be precisely control by syringe infusion pump. It is designed in such a way that the flow mechanism through the pipe match to the extent, as the sap flows in the natural plant. Virtual plant model consists of a syringe infusion pump (LPM-50DN), medical syringe and a PVC pipe. To get the proper output signals from the sensor, the outer diameter of the PVC pipe must match with the stem diameter of the sensor, otherwise the reading will be erroneous because of insufficient and uneven heating. To vary the flow rate through the virtual plant we can either change the flow rate of the syringe infusion pump or we can change the syringe of different volume. These are following components used to construct the virtual plant:

- Syringe infusion pump
- PVC pipe
- Medical syringe

## 2.5.1 Syringe Infusion Pump (LPM-50DN)

A syringe infusion pump is a medical device used to deliver fluids into a patient's body in a precisely controlled manner. There are many different types of infusion pumps, which are used for a variety of purposes and in a variety of environments.

Infusion pumps may be capable of delivering fluids in large or small amounts, and may be used to deliver nutrients or medications – such as insulin or other hormones, antibiotics, chemotherapy drugs, and pain relievers.

LPM-50DN micro-infusion syringe pump is a portable & unique apparatus, specially designed to deliver fluids into a patient's body with superior accuracy.

### Features:

- Rate mode, time mode, volume mode
- LED & LCD Display
- Regulating flow rate conveniently
- Automatically recognize syringe size & brand
- Audio and video & voice alarm
- Total volume indicator



Figure 2.3: Syringe infusion pump

## 2.5.2 PVC Pipe

To design the virtual plant we used the PVC pipe as a stem of the virtual plant model. The inner and the outer diameter of the pipe are 4 mm and 5.5 mm respectively. Two types of syringes have been used in designing the virtual plant. The first syringe is of 5 ml which is shown the first figure below and another diameter of 10 ml, which is installed in the syringe infusion pump to complete the design of virtual plant.



Figure 2.4: PVC pipe of 5 mm diameter



### 2.5.3 Medical Syringe and Virtual Plant Model.



Figure 2.5: 5 ml Syringe and Virtual plant model



## 2.6 Design of the Amplifier

The sap sensor mainly consists of thermocouples, thermopiles and the heater element. The output readings from the sensor come from the two thermocouples and one thermopile, and we know that signals from the TC and the thermopile are very small in magnitude. So in order to do the measurement through the data acquisition card we need to amplify the output signals coming from the sensor. These are the following components used to design the amplifier.

- Operational amplifier (AD 8630)
- Resistors
- Breadboard
- Power supply

### 2.6.1 Operational Amplifier (AD 8630)

This AD 8630 amplifier has ultralow offset, drift, and bias current. The AD8630 is wide bandwidth auto-zero amplifiers featuring rail-to-rail input and output swing and low noise. Operation is fully specified from 2.7 V to 5 V single supply ( $\pm 1.35$  V to  $\pm 2.5$  V dual supply).

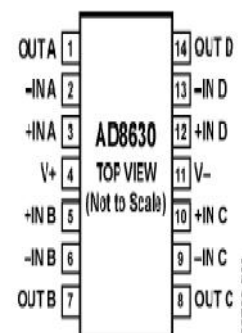
With an offset voltage of only 1  $\mu$ V, drift of less than 0.005  $\mu$ V/ $^{\circ}$ C, and noise of only 0.5  $\mu$ V p-p (0 Hz to 10 Hz), AD8630 are suited for applications where error sources cannot be tolerated. Position and pressure sensors, medical equipment, and strain gage amplifiers benefit greatly from nearly zero drift over their operating temperature range. Many systems can take advantage of the rail-to-rail input and output swings provided by the AD8630 to reduce input biasing complexity and maximize SNR.

#### Features

- Lowest auto-zero amplifier noise
- Low offset voltage: 1  $\mu$ V
- Input offset drift: 0.002  $\mu$ V/ $^{\circ}$ C
- Rail-to-rail input and output swing
- 5 V single-supply operation
- High gain, CMRR, and PSRR: 130 dB
- Very low input bias current: 100 pA maximum

#### Application

- Pressure and position sensors
- Strain gage amplifiers
- Medical instrumentation
- Thermocouple amplifiers
- Precision current sensing
- Photodiode amplifiers



14-LEAD STANDARD SMALL OUTLINE PACKAGE [SOIC\_N]  
NARROW BODY (R-14)  
14-LEAD THIN SHRINK SMALL OUTLINE PACKAGE [TSSOP]  
(RU-14)

Figure 2.6: AD8630 TOP VIEW

## 2.6.2 Amplifier Circuit Diagram

Three amplifier circuits have been designed to amplify the signals coming from the sensor. All the amplifiers are non-inverting amplifier which has been designed with the help of two resistors and one operational amplifier. Op-Amp (AD 8630) has been used because it has certain advantages over the other operational amplifiers. The resistor used in the feedback path is a variable resistor, so that the gain of the amplifier can be changed whenever required.

The gain of the amplifier is

$$V_{out} \approx 1 + \frac{R_f}{R_{in}} \quad (2.1)$$

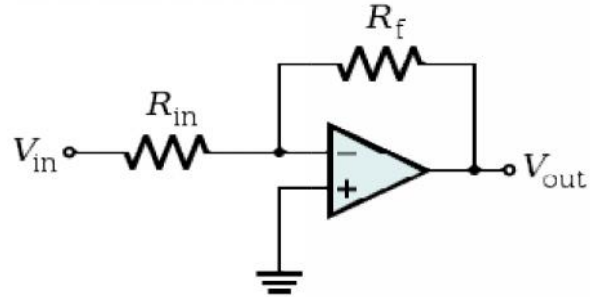


Figure 2.7: Noninverting Amplifier

## 2.7 Stem Heat Balance Theory and Working Equations

The SHB method requires a steady state and a constant energy input from the heater strip inside the gage body. Therefore the stem section must be insulated from changes in the environment. For the same reason, the gage time constant is limited from five minutes to an hour, depending on the flow rate and the stem size. Figure 2.8 shows a stem section and the possible components of heat flux, assuming no heat storage. The heater surrounds the stem under test and is powered by a DC supply with a fixed amount of heat ( $Q_h$ ).  $Q_h$ , is the equivalent to the power input ( $P_{in}$ ) to the stem from the heater.  $Q_r$ , is the radial heat conducted through the gage to the ambient.  $Q_v$ , the vertical or axial heat conduction through the stem has two components,  $Q_u$  and

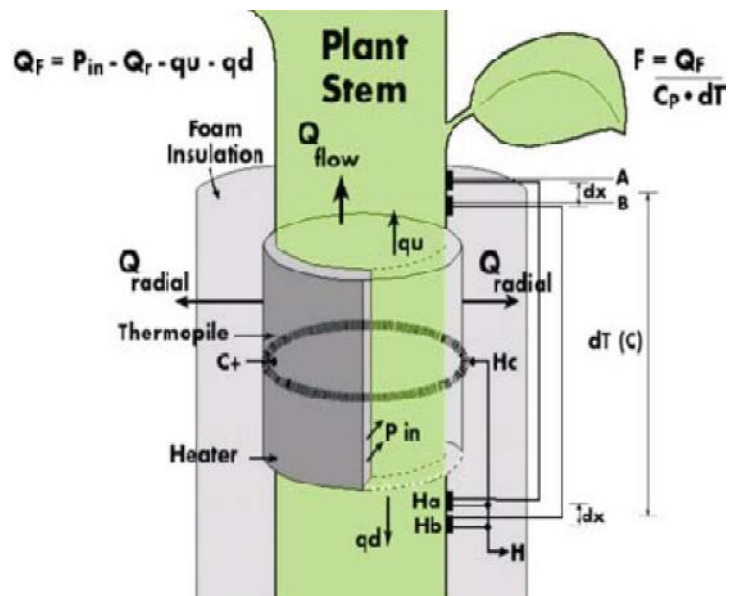


Figure 2.8: Stem Gage Schematics

$Q_d$ . By measuring  $P_{in}$ ,  $Q_u$ ,  $Q_d$ , and  $Q_r$ , the remainder,  $Q_f$  can be calculated.  $Q_f$  is the heat convection carried by the sap. After dividing by the specific heat of water and the sap temperature increase, the heat flux is converted directly to mass flow rate.

### 2.7.1 Working Equations:

The energy balance is expressed as:

$$P_{in} = Q_r + Q_v + Q_f \quad (W) \quad (2.2)$$

$$\text{where, } P_{in} = \frac{V^2}{R}$$

Fourier's Law describes the vertical conduction components:

$$Q_v = Q_u + Q_d \quad (2.3)$$

$$\text{Where } Q_u = K_{st} A \frac{dT_u}{dX} \quad (2.4)$$

$$Q_d = K_{st} A \frac{dT_d}{dX} \quad (2.5)$$

Where  $K_{st}$  is the thermal conductivity of the stem (W/m·K),  $A$  is the stem cross-sectional area ( $m^2$ ); the temperature gradients are  $dT_u / dX$  (K/m) and  $dT_d / dX$ ;  $dX$  is the spacing between thermocouple junctions ( $m$ ). One pair of thermocouples is above the heater and one pair is below the heater as shown on the schematic in Figure 2.9. There are two differentially wired thermocouples both measuring the rise in sap temperature. Channel AH measures the difference in temperature  $A - H_a$  (mV). Channel BH measures the difference in temperature  $B - H_b$  (mV).

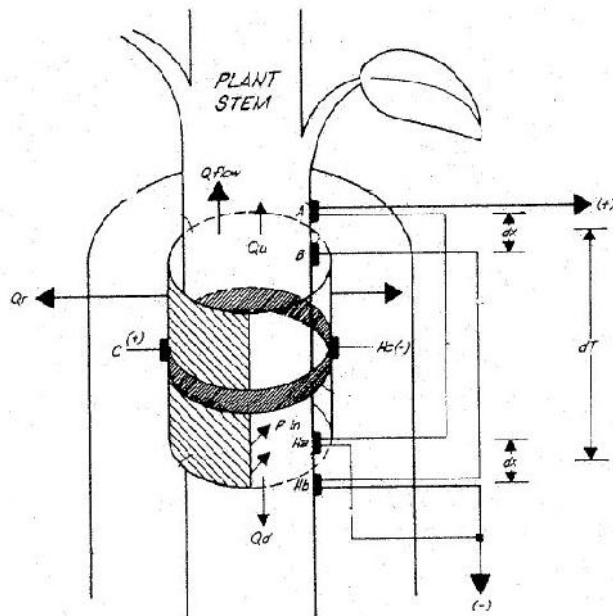


Figure 2.9: Thermocouple and heater in Dynagage

By subtraction of these two signals:

$$BH - AH = (B - H_b) - (A - H_a) = (B - A) + (H_a - H_b) \quad (\text{mV}) \quad (2.6)$$

The result yields the two components of axial heat conduction out of the stem section,  $Q_u$  and  $Q_d$  (See Fig. 2.9). Since the distances separating the upper TC pair and lower TC pair is fixed by design for each particular gage to the same value, the components of  $Q_v$  are combined with a common denominator:

$$Q_v = \frac{K_{st} \times A \times (BH - AH)}{dX \times .040 \text{mV}/C} \quad (\text{W}) \quad (2.7)$$

The factor .040 mV/C converts the thermocouple differential signals to degrees C.  $K_{st}$  values, which is the thermal conductivity of the stem W/m.K, are given for the PVC pipe is 0.19 W/m.K

## 2.7.2 Sap Thermodynamics Equations

Rearranging the equation (2.2)

$$Q_f = P_{in} - Q_v - Q_r \quad (\text{W}) \quad (2.8)$$

When we divide the  $Q_f$  by the specific heat of water and the sap temperature increase, the heat flux is directly converted to mass flow rate.

$$F = \frac{Q_f}{C_p \times dT} = \frac{P_{in} - Q_v - Q_r}{C_p \times dT} \quad (\text{Gram/sec}) \quad (2.9)$$

In equation (2.8) the radial heat loss is computed in by,

$$Q_r = K_{sh} \times CH \quad (\text{W}) \quad (2.10)$$

$K_{sh}$  is the thermal conductance constant for a particular gage installation.  $C_p$  is the specific heat of water (4.186 J/g·C), and  $dT$  is the temperature increase of the sap. The temperature increased in the sap;  $dT$  is measured in mV by averaging AH and BH signals and then converted to °C by dividing by the thermocouple temperature conversion constant.

$$dT = \frac{(AH + BH)/2}{.040 \text{mV}/^\circ\text{C}} \quad (^\circ\text{C}) \quad (2.11)$$

### 2.7.3 Apparent $K_{sh}$ Calculation

To calculate the  $Q_r$ , we need to calculate  $K_{sh}$  first, and  $K_{sh}$  is determined by solving equation (2.10)

When setting  $Q_f = 0$ , eq. (2.2) reduces to

$$P_{in} = Q_r + Q_v \quad (\text{W}) \quad (2.12)$$

Rearranging eq. (2.12)

$$Q_r = P_{in} - Q_v \quad (\text{W}) \quad (2.13)$$

We know from eq. (2.10)

$$Q_r = K_{sh} \times CH \quad (\text{W}) \quad (2.14)$$

Equating eq. (2.13) and eq. (2.14), we get

$$K_{sh} = \frac{P_{in} - Q_v}{CH} \quad (\text{W} / \text{mV}) \quad (2.15)$$

Once we compute  $K_{sh}$  then  $Q_r$  can be simply calculated using the equation (2.10).

### 2.7.4 Steps to be followed to compute the flow rate F

Step 1

Calculate the sheath conductance  $K_{sh}$  with the no flow condition i.e.,  $F = 0$  using equation (2.15)

Step 2

Calculate the radial heat conduction  $Q_r$  using equation (2.10)

Step 3

Calculate the vertical or axial heat conduction  $Q_v$  using equation (2.3)

Step 4

Calculate the heat convection  $Q_f$  using equation (2.8)

Step 5

Calculate the temperature increase in the sap  $dT$  using equation (2.11)

Step 6

Calculate the mass flow rate  $F$  using equation (2.9)

\*\*\*\*\*

## Chapter 3

In this chapter we will talk about the different type of configuration of virtual plant model which we have designed to perform the different experiments. We will also talk about the problems faced during the measurements and its remedy in further experiments. Thereafter, we will see the results and discussions at the end of each experiment and we will also talk about the reason behind to perform every experiment and how we may further improve the experimental results and what should be the basic approach to increase the operating span of the Virtual Plant Model in the next to the previous experiment. In the end of this chapter we will see the conclusion about the complete work and we will also talk about the future scope of this work in brief.

### 3.1 Experiment No:-1

Our first objective was to investigate the virtual plant model about its behavior and the working range. Therefore, we haven't amplified the signals rather than we have taken measurements directly from the sensor with the help of 4 and ½ digit voltmeter. We have taken the measurements corresponding to the virtual plant model shown in the Fig 3.1. The readings are shown for the different parameters in the table 3.1

Table 3.1: Readings taken in the interval of 30 minutes using 20 ml syringe on 2nd march 2016

CH (mv)	BH (mv)	AH (mv)	Vin (volt)	Pin (watt)	Actual flow (ml/h)
0.36	0.12	-0.03	4.0	0.093	0.5
0.35	0.13	-0.01	4.0	0.093	1.0
0.34	0.14	0.00	4.0	0.093	1.5
0.33	0.15	0.01	4.0	0.093	2.0
0.32	0.16	0.02	4.0	0.093	2.5
0.31	0.17	0.03	4.0	0.093	3.0
0.30	0.18	0.03	4.0	0.093	3.5
0.30	0.19	0.04	4.0	0.093	4.0

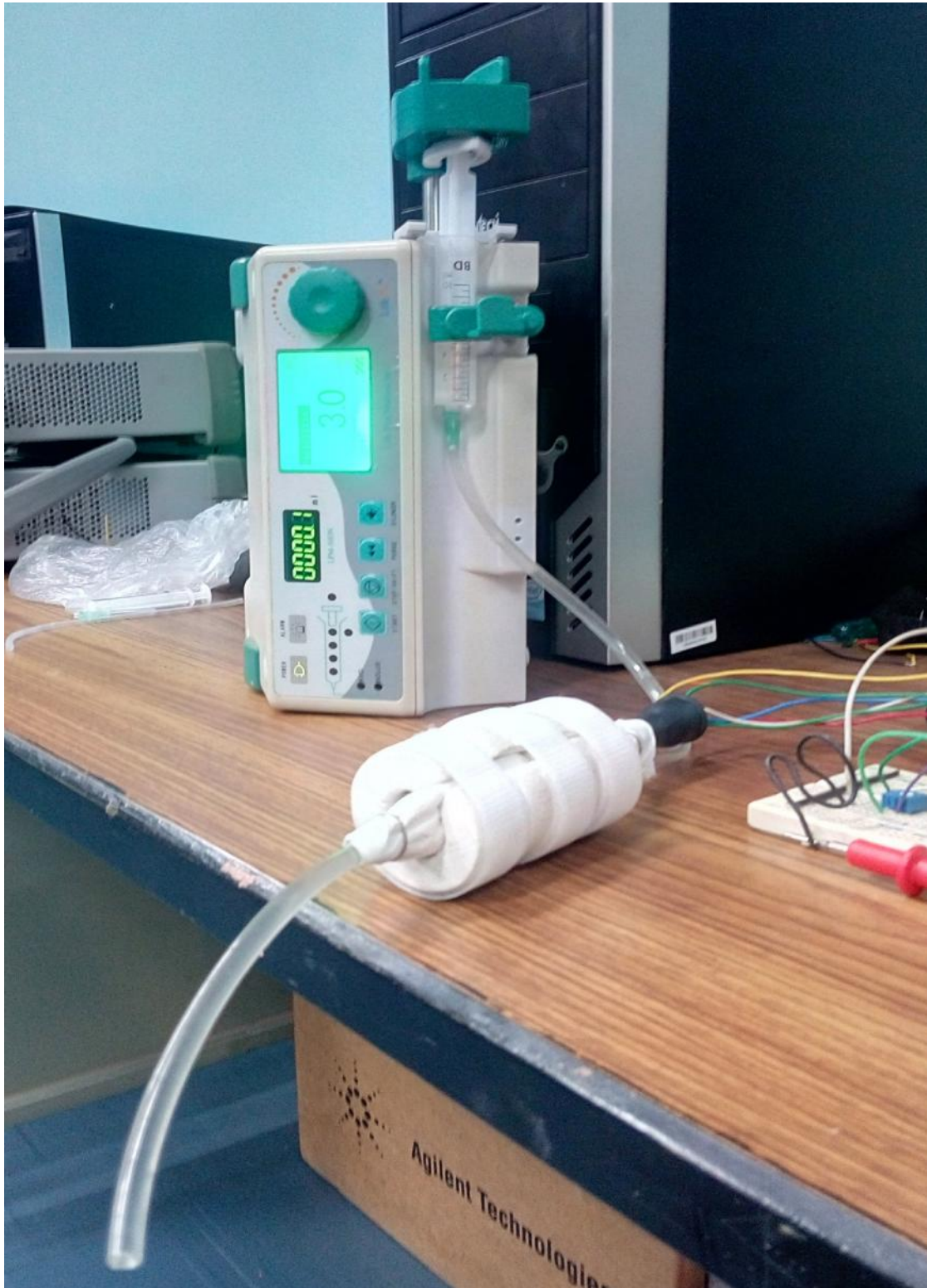


Figure 3.1: See how the sensor is installed in the stem of virtual plant model for performing the experiment

Table 3.2: Readings taken in the interval of 30 minutes using 20 ml syringe on 3rd march 2016

CH (mv)	BH (mv)	AH (mv)	Vin (volt)	Pin (watt)	Actual flow (ml/h)
0.36	0.07	-0.07	4.0	.093	0.5
0.36	0.08	-0.05	4.0	.093	1.0
0.36	0.09	-0.04	4.0	.093	1.5
0.35	0.10	-0.03	4.0	.093	2.0
0.35	0.11	-0.02	4.0	.093	2.5
0.35	0.12	-0.01	4.0	.093	3.0
0.34	0.14	0.00	4.0	.093	3.5
0.34	0.14	0.00	4.0	.093	4.0

Table 3.3: Readings taken in the interval of 30 minutes using 20 ml syringe on 8th march 2016

CH (mv)	BH (mv)	AH (mv)	Vin (volt)	Pin (watt)	Actual flow (ml/h)
0.35	0.09	-0.05	4.0	.093	0.5
0.35	0.09	-0.05	4.0	.093	1.0
0.34	0.08	-0.04	4.0	.093	1.5
0.33	0.10	-0.04	4.0	.093	2.0
0.33	0.11	0.00	4.0	.093	2.5
0.32	0.12	0.00	4.0	.093	3.0
0.31	0.13	0.01	4.0	.093	3.5
0.31	0.13	0.01	4.0	.093	4.0

### 3.1.1 Results and Discussions:

We have taken the readings in the table 3.1 and table 3.2 with the same virtual plant model as shown in the Fig. 3.1. The only difference is that we have taken these readings on different days to test the repeatability. As we can see that the virtual plant is same but we are getting different signals with the same flow rate. Therefore, it is difficult to say which readings are accurate, or we can say that its repeatability is not good. Thus, to the test the repeatability of the measured data we have taken further readings which are shown in table 3.3. Now by looking at the table 3.1, 3.2 and table 3.3, it can be clearly seen that readings are not the same, even not close to the other reading. So by observing all the data available to us, we might conclude at this moment that we need to take the measurements with some other configuration of the virtual plant model so that the results can be improved.



## 3.2 Experiment No:-2

In this experiment we have made two changes, the first change in the configuration of the virtual plant model as shown in the Fig. 3.1, is in the syringe volume, where we have used 5 ml syringe to reduce the flow rate and the second change is in the heater input. In the previous experiment we applied 4.0 V to the heater input but here we applied 4.2 V for the proper functioning of the heater as recommended by the sensor manufacturer. The measured readings are shown in the table 3.4

Table 3.4: Readings taken in the interval of 30 minutes using 5 ml syringe on 9th march 2016

CH (mv)	BH (mv)	AH (mv)	Vin (volt)	Pin (watt)	Actual flow (ml/h)
0.28	0.04	-.03	4.2	.103	0.2
0.27	0.04	-.03	4.2	.103	0.4
0.27	0.04	-.03	4.2	.103	0.6
0.28	0.04	-.03	4.2	.103	0.8
0.28	0.05	-.02	4.2	.103	1.0
0.27	0.07	0.01	4.2	.103	4.0
0.23	0.08	0.01	4.2	.103	8.0
0.21	0.09	0.03	4.2	.103	12.0

### 3.2.1 Results and Discussions:

In the table 3.4 we can see that CH varies according to the change in the flow rate but observing BH and AH, there is no change in the BH and AH when the flow rate changes from 0.2 ml/h to 0.8 ml/h. So even with this experiment, we are not getting the satisfactory result; that means actually CH, BH and AH must change when the flow rate changes. One of the cause of not varying the BH and AH signals may be the extreme low flow rate i.e., the resolution of the sap flow sensor is not good as require to detect the extreme low flow rate. Therefore we may have to increase the flow rate more than 1 ml/h in one step so that the sap flow sensor might detect the flow and we may get the variation in the BH and AH or we may have to further improve the flow mechanism through the PVC pipe such that water flowing through the pipe should match exactly as the sap flow in any natural plant.

### 3.3 Experiment No:-3

In this experiment our main objective was to design the stem of the virtual plant model such that the water flowing through the pipe must match to some extent, as the sap flows in the natural plant or trees. “In order to do so, we have inserted an outer diameter of 3 mm pipe into an inner diameter of 4 mm pipe” to construct a layer of 1 mm between the two pipes and then we have blocked one of the end of the inner pipe so that water doesn’t flow through the inner pipe. We have connected the syringe to the pipe such that the water flows, only to the outer layer of the inner pipe and thereby reducing the volume of the water so that the water flowing through the layer gets more heat in order to get more temperature variation between two thermocouple junctions and in this way we might get the better readings than the previous experiments. The data in the table 3.5 are shown based on the experiment number 3.

Table 3.5: Readings taken in the interval of 30 minutes using 20 ml syringe on 10th march 2016

CH (mv)	BH (mv)	AH (mv)	Vin (volt)	Pin (watt)	Actual flow (ml/h)
0.27	.03	-.02	4.2	.103	0.0
0.23	0.13	0.06	4.2	.103	5.0
0.22	0.13	0.06	4.2	.103	6.0
0.21	0.13	0.07	4.2	.103	7.0
0.20	0.12	0.06	4.2	.103	8.0
0.19	0.12	0.05	4.2	.103	9.0
0.18	0.11	0.04	4.2	.103	10.0
0.17	0.08	0.03	4.2	.103	15.0
0.15	0.07	0.02	4.2	.103	20.0
0.15	0.05	0.01	4.2	.103	30.0
0.14	0.04	0.00	4.2	.103	50.0

#### 3.3.1 Computation of the Flow Rate F

These are the following constants which we have used to determine the practical flow rate F.

Radius of the stem of the virtual plant= 2.5mm

$$\begin{aligned} \text{Cross-sectional area of the virtual plant (A)} &= \pi r^2 \\ &= 1.9634 \times 10^{-5} \text{ m}^2 \end{aligned}$$

Specific heat of water  $C_p = 4.1813 \text{ J}/(\text{g} \cdot ^\circ\text{C})$

Resistance of the heater,  $R = 171\Omega$

TC Gap  $dX = 3\text{mm}$

Thermal conductivity of the PVC pipe,  $K_{st} = .19 \text{ W}/(\text{m} \cdot ^\circ\text{C})$

Voltage applied to the heater,  $V = 4.2 \text{ volt}$

Pin (watt)  $= .103 \text{ W}$

### 3.3.2 Calculation of sheath conductance:

Using eq. (2.15) and (2.7), and putting all the constants in the respective equation,  $K_{sh}$  is calculated as

$$K_{sh} = .3803 \text{ W}/(\text{mV})$$

Note: - The sheath conductance is calculated when we have established a no-flow condition i.e., when  $F = 0$ .

After calculating the sheath conductance ( $K_{sh}$ ), we have used the steps as explained in the section 2.7.4 to determine the practical flow rate ( $F$ ), for the respective data we have taken during the measurement, which is shown in table 3.5. The measured flow rate ( $F$ ), is shown in the table 3.6, in addition with that all the parameters prior to the calculations of practical flow rate are also shown in the same table.

Table 3.6: Actual flow rate versus measured flow rate

CH	BH	AH	Vin	Pin	$Q_v$	$Q_r$	$Q_f$	dT	$K_{sh}$	Actual flow rate	Measured flow rate
(mv)	(mv)	(mv)	volts	W	W	W	W	$^\circ\text{C}$	W/mv	ml/h	gm/h
0.23	0.13	0.06	4.2	.103	.00217	.08747	.01335	2.375	.3803	5.0	4.839
0.22	0.13	0.06	4.2	.103	.00217	.08366	.01716	2.375	.3803	6.0	6.220
0.21	0.13	0.07	4.2	.103	.00186	.07980	.02133	2.500	.3803	7.0	7.340
0.20	0.12	0.06	4.2	.103	.00186	.07606	.02507	2.250	.3803	8.0	9.590
0.19	0.12	0.05	4.2	.103	.00217	.07226	.02856	2.125	.3803	9.0	11.57
0.18	0.11	0.04	4.2	.103	.00217	.0684	.03243	1.875	.3803	10.0	14.89
0.17	0.08	0.03	4.2	.103	.00155	.0646	.03684	1.375	.3803	15.0	23.02
0.15	0.07	0.02	4.2	.103	.00155	.05704	.04441	1.125	.3803	20.0	33.98
0.15	0.05	0.01	4.2	.103	.05704	.01243	.04471	.7500	.3803	30.0	51.33
0.14	0.04	0.00	4.2	.103	.00124	.05320	.04855	.5000	.3803	50.0	83.60

Table 3.7: Error between actual flow rate and measured flow rate

Actual flow rate	Measured flow rate	Error	Result
ml/h	gm/h	%	
5.0	4.839	3.22	✓
6.0	6.220	3.66667	✓
7.0	7.340	4.85714	✓
8.0	9.590	19.875	✓
9.0	11.57	28.5556	✗
10.0	14.89	48.9	✗
15.0	23.02	53.4667	✗
20.0	33.98	69.9	✗
30.0	51.33	71.1	✗
50.0	83.60	67.2	✗

### 3.3.3 Results and discussions:

By looking in the table 3.6, we can see that measured flow rate is very close to the actual flow rate from 5 ml/h to 8 ml/h, and as the actual flow rate increases further, error in the measured flow rate also increases exponentially. So by comparing the measured flow rates with the actual flow rate as shown in the table 3.7, we can infer that the design of virtual plant model based on the experiment 3 is working quite well for the flow rate from 5 ml/h to 8 ml/h. we may also notice from the table 3.7, that we haven't achieved very satisfactory result for the higher flow rate but its operation is quite good for the medium range (5 ml/h to 8 ml/h). One of the reasons of not working properly for higher flow rate might be the operating range of the sensor i.e., the flow rate might be exceeding beyond the capability of sensor operating range. Therefore, we might have to change the sensor and or we still need to look for some other design of the virtual plant model to get the result with greater accuracy and improving its operating range. Since, we have only one sensor so there is no question of replacing the sensor with higher operating range. Therefore, we must have to go for the second option i.e., we have to further modify the design of the virtual plant and performing the next experiment.

## Comparison between Actual flow rate and calculated flow rate

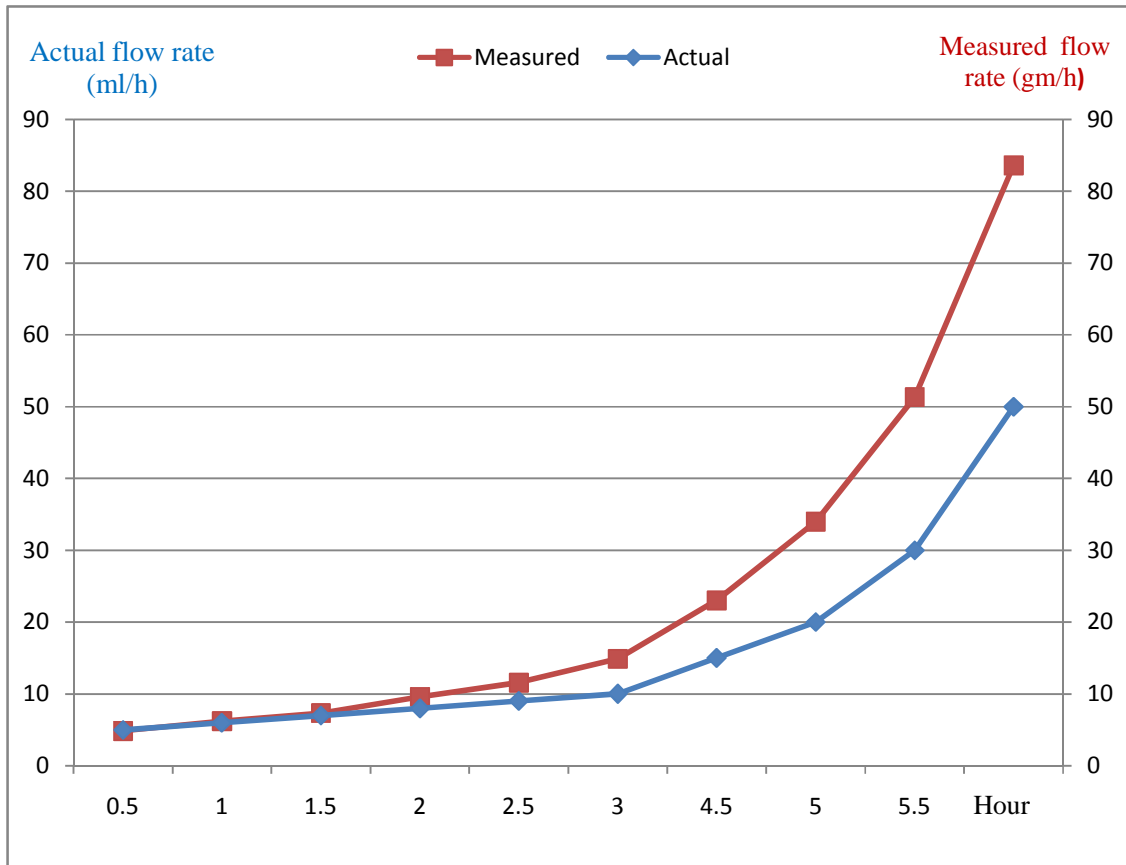


Figure 3.2: Sap-flow rate analysis

In the figure 3.3, the graph for the change in temperature versus measured flow rate is shown and from the graph we can see that as the flow rate increases, change in temperature decreases continuously. Therefore we can infer that change in temperature is inversely proportional to the flow rate.

In figure 3.4, the plot of different heat flux profiles are shown, and we can see that the radial conduction  $Q_r$  plays an important role because most of the input heat energy is lost in the radial direction, while we can also see that magnitude of the vertical heat conduction  $Q_v$  is the minimum.

### Sap Flow Analysis

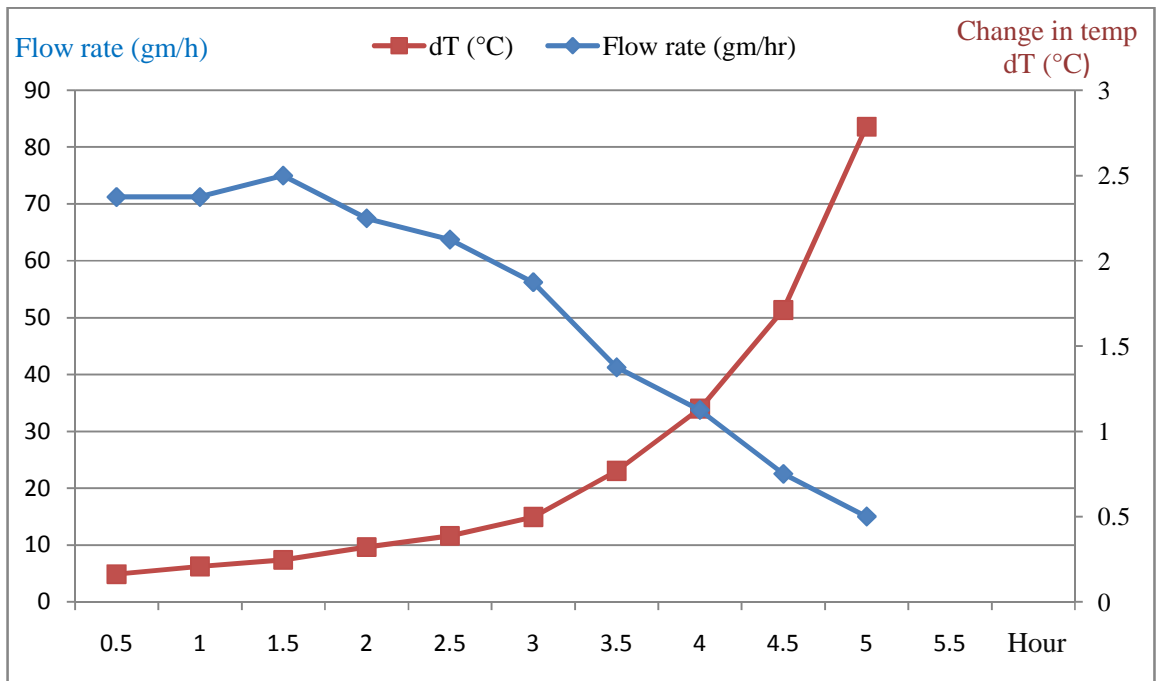


Figure 3.3: Change in temperature versus Flow rate

### Heat flux (W) Analysis

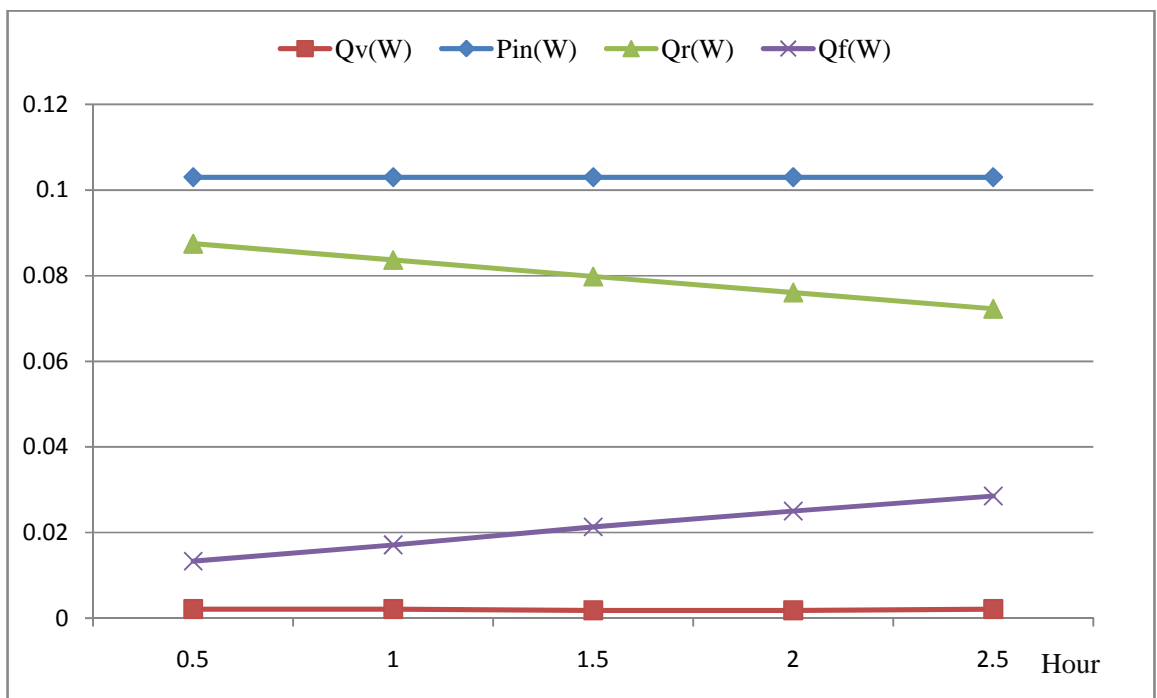


Figure 3.4: Heat flux analysis

### 3.4 Experiment No:-4

As we have seen in the experiment no. 3, the design of the virtual plant model hasn't given the satisfactory results for higher flow rates, which lead us to perform another experiment. In this experiment, we used again a single PVC pipe of diameter 5 mm (as we have used in the experiment no. 1) as the stem of the virtual plant model, and more importantly, we have changed the orientation of the stem which is a major change comparing to all earlier experiments. In all the earlier experiments we have used the stem which was placed horizontally (see Fig. 3.1) and the sensor was also installed horizontally but in this experiment we have arranged the pipe (stem of the virtual plant model) such that water flow through the pipe in the direction from bottom to

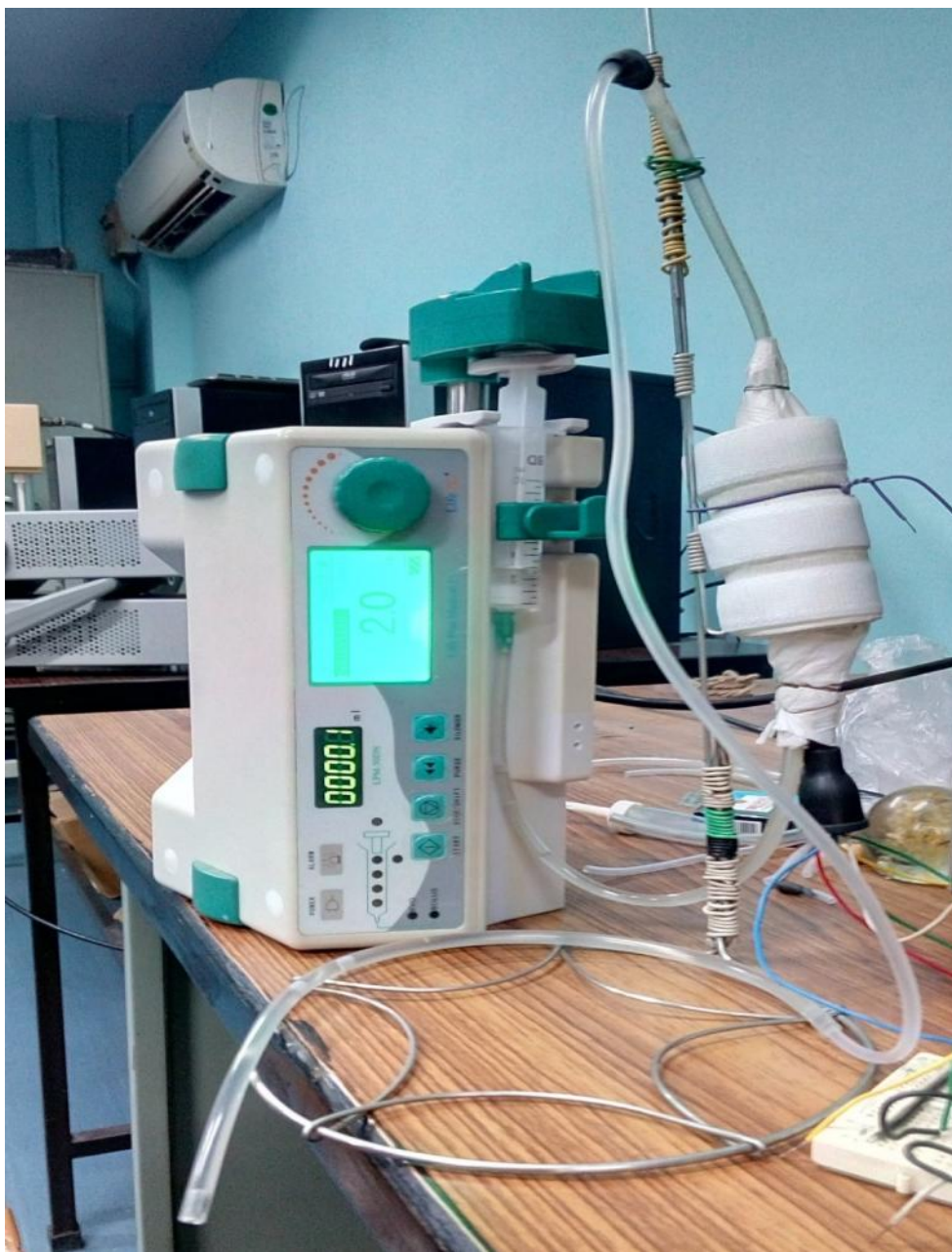


Figure 3.5: Sensor installation in the vertical direction

top, as the sap flows in any natural plant and we have also installed the sensor vertically. Note that the correct end of the gage should be up, that is toward the plant apex i.e., *the sap flow direction is up when the cable connector points down*. This is recommended by the sensor's manufacturer. The other change was in the applied voltage to the heater. The complete measurement set up is shown in the Fig. 3.5 and readings are shown in the table 3.8

Table 3.8: Readings taken in the interval of 30 minutes using 20 ml syringe on 6th April 2016

CH (mv)	BH (mv)	AH (mv)	Vin (volt)	Pin (watt)	Actual flow (ml/h)
.253	.062	-.025	4.020	.09456	0
.254	.079	-.010	4.020	.09456	1
.257	.108	.017	4.020	.09456	2
.250	.128	.044	4.020	.09456	3
.238	.140	.063	4.020	.09456	4
.224	.142	.072	4.020	.09456	5
.210	.138	.073	4.020	.09456	6
.200	.128	.068	4.020	.09456	7
.196	.130	.070	4.020	.09456	8
.184	.112	.058	4.020	.09456	9
.178	.104	.053	4.020	.09456	10
.171	.099	.049	4.020	.09456	11
.167	.094	.047	4.020	.09456	12

### 3.4.1 Calculation of sheath conductance:

Again, using eq. (2.15) and (2.7), and putting all the constants in the respective equation,  $K_{sh}$  is calculated as

$$K_{sh} = .3692 \text{ W / (mV)}$$

Note: - The sheath conductance is calculated when we have established a no-flow condition i.e., when  $F = 0$ .

After calculating the sheath conductance ( $K_{sh}$ ), we have used the steps as explained in the section 2.7.4 to determine the practical flow rate ( $F$ ), for the respective data we have taken during the measurement, which is shown in table 3.8. The measured flow rate ( $F$ ), is shown in the table 3.9, in addition with that all the parameters prior to the calculations of practical flow rate are also shown in the same table.



Table 3.9: Actual flow rate versus measured flow rate

CH	BH	AH	V <sub>in</sub>	Q <sub>v</sub>	Q <sub>r</sub>	Q <sub>f</sub>	dT	K <sub>sh</sub>	Actual flow rate	Measured flow rate
(mv)	(mv)	(mv)	volts	W	W	W	°C	W/mv	ml/h	gm/h
0.254	-0.01	0.079	4.020	0.0028	0.0938	-0.002	0.8625	0.3692	1	-1.98
0.257	0.017	0.108	4.020	0.0028	0.0949	-0.003	1.5625	0.3692	2	-1.74
0.250	0.044	0.128	4.020	0.0026	0.0923	-0.001	2.1500	0.3692	3	-0.14
0.238	0.063	0.140	4.020	0.0024	0.0879	0.0043	2.5375	0.3692	4	1.46
0.224	0.072	0.142	4.020	0.0022	0.0827	0.0097	2.6750	0.3692	5	3.11
0.210	0.073	0.138	4.020	0.0020	0.0775	0.0150	2.6375	0.3692	6	4.89
0.200	0.068	0.128	4.020	0.0019	0.0738	0.0189	2.4500	0.3692	7	6.62
0.196	0.070	0.130	4.020	0.0019	0.0724	0.0203	2.5000	0.3692	8	6.99
0.184	0.058	0.112	4.020	0.0017	0.0679	0.0249	2.1250	0.3692	9	10.10
0.178	0.053	0.104	4.020	0.0016	0.0657	0.0273	1.9625	0.3692	10	11.94
0.171	0.049	0.099	4.020	0.0016	0.0631	0.0299	1.8500	0.3692	11	13.89
0.167	0.047	0.094	4.020	0.0015	0.0617	0.0314	1.7625	0.3692	12	15.34

Table 3.10: Error between actual flow rate and measured flow rate

Actual flow rate	Measured flow rate	Error	Result
ml/h	gm/h	%	
4	1.46	63.5	✘
5	3.11	37.8	✘
6	4.89	18.5	✓
7	6.62	5.428571	✓
8	6.99	12.625	✓
9	10.10	12.2222	✓
10	11.94	19.4	✓
11	13.89	26.2727	✘
12	15.34	27.8333	✘

### 3.4.2 Results and discussions:

In the table 3.9, we can see that for the actual flow rate 1 ml/h to 3 ml/h we are getting measured flow rate in negative and when the flow rate is increased to 4 ml/h we are getting measured flow rate 1.46 gm/h. We can also notice that as we increase the actual flow rate from 4 ml/h, error between the actual and the measured flow rate reduces up to 9 ml/h and when the actual flow rate increases further from 9 ml/h error starts increasing. It can be seen in the table 3.10, that the lowest percentage error is corresponding to the flow rate 7 ml/h, where the error is only 5.42 %. Therefore, again it is clear that designed virtual plant model based on experiment no. 4 is failed to measure higher flow rate successfully. Therefore, we can conclude that our design is only giving satisfactory result for 6 gm/h to 10 gm/h and it cannot be used for any other flow rate and to measure, especially the higher flow rate with this configuration we may have to replace the sensor with higher operating range.

In Fig. 3.6, we can see that heat flux have the similar pattern as we have seen in the previous experiment and in Fig. 3.8, again the maximum heat is lost in the radial direction, and  $Q_v$  has the minimum magnitude.

#### Comparison between Actual flow rate and calculated flow rate

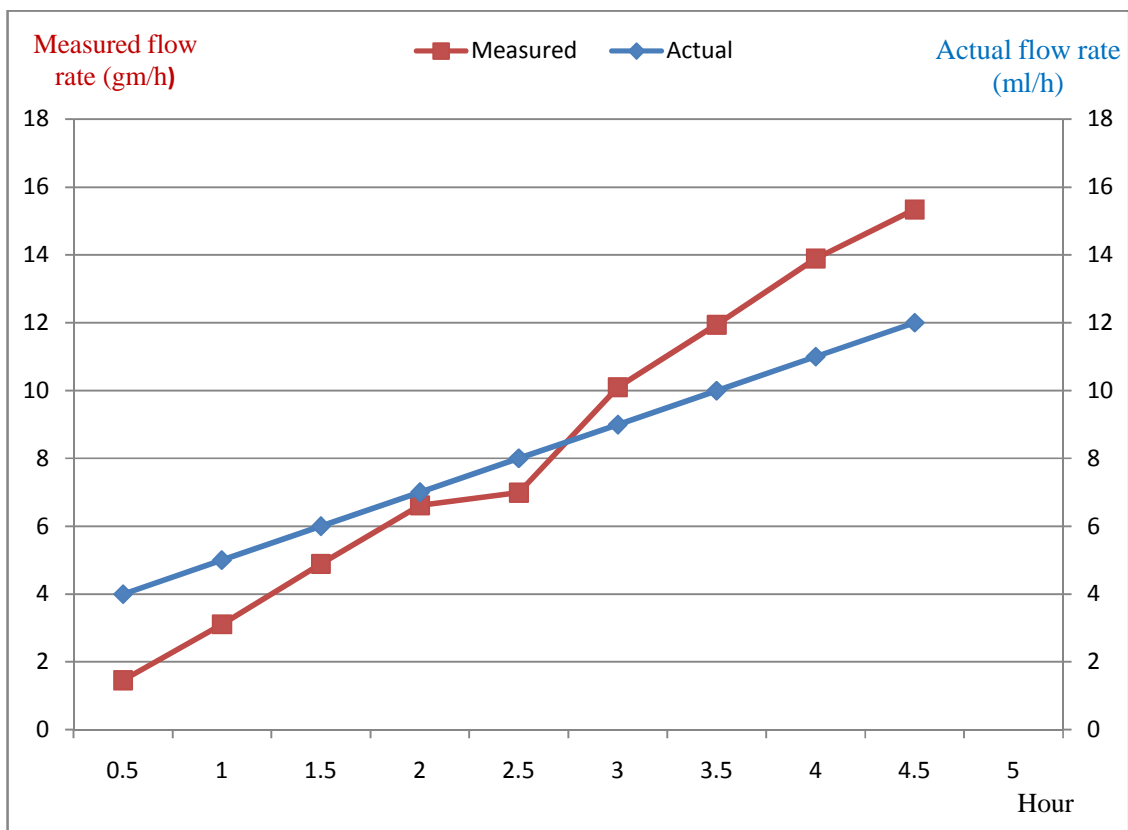


Figure 3.6: Sap flow rate analysis

### Sap Flow Analysis

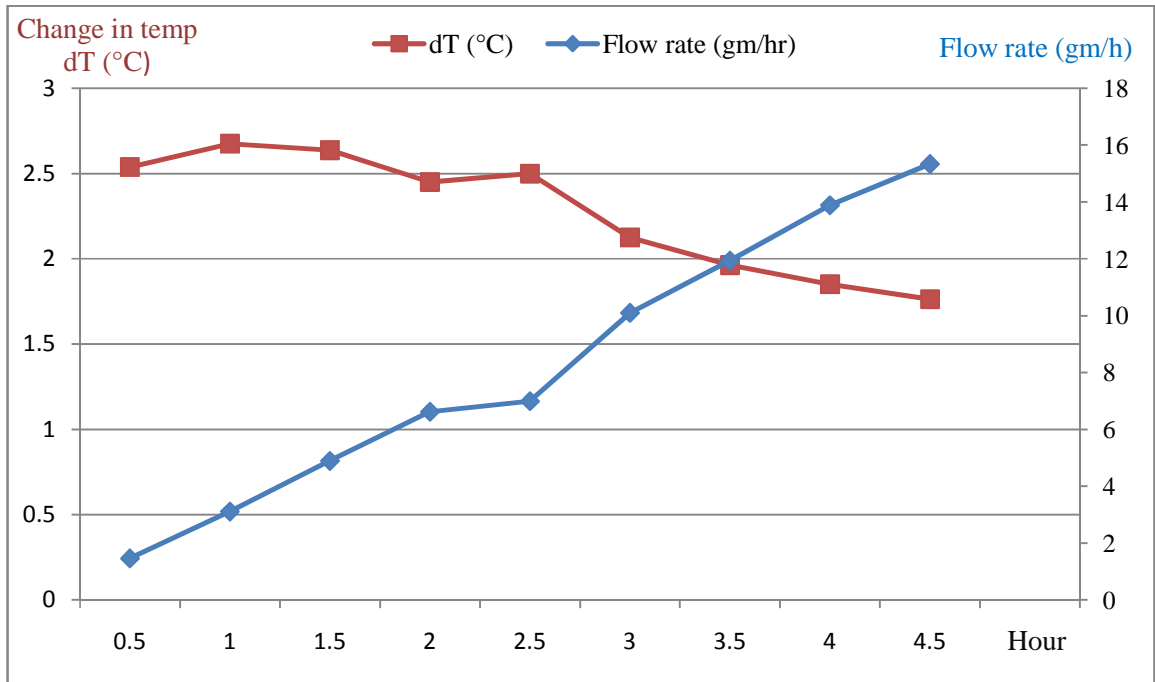


Figure 3.7: Change in temperature versus Flow rate

### Heat flux (W) Analysis

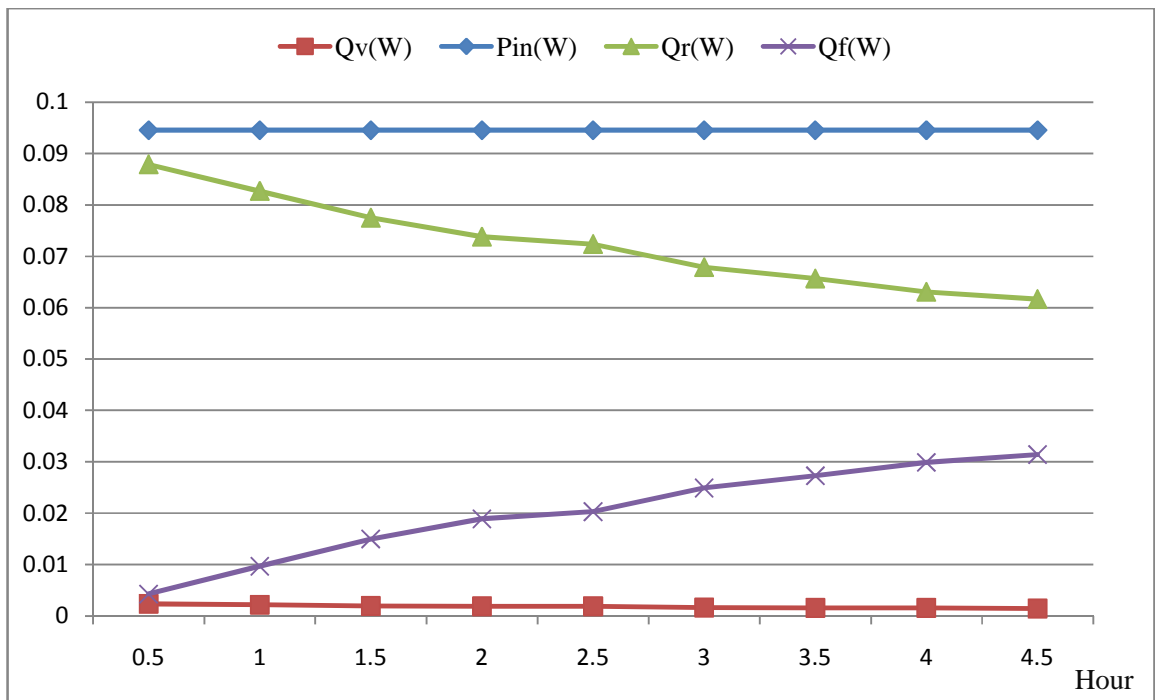


Figure 3.8: Heat flux analysis

### Calibration Curve

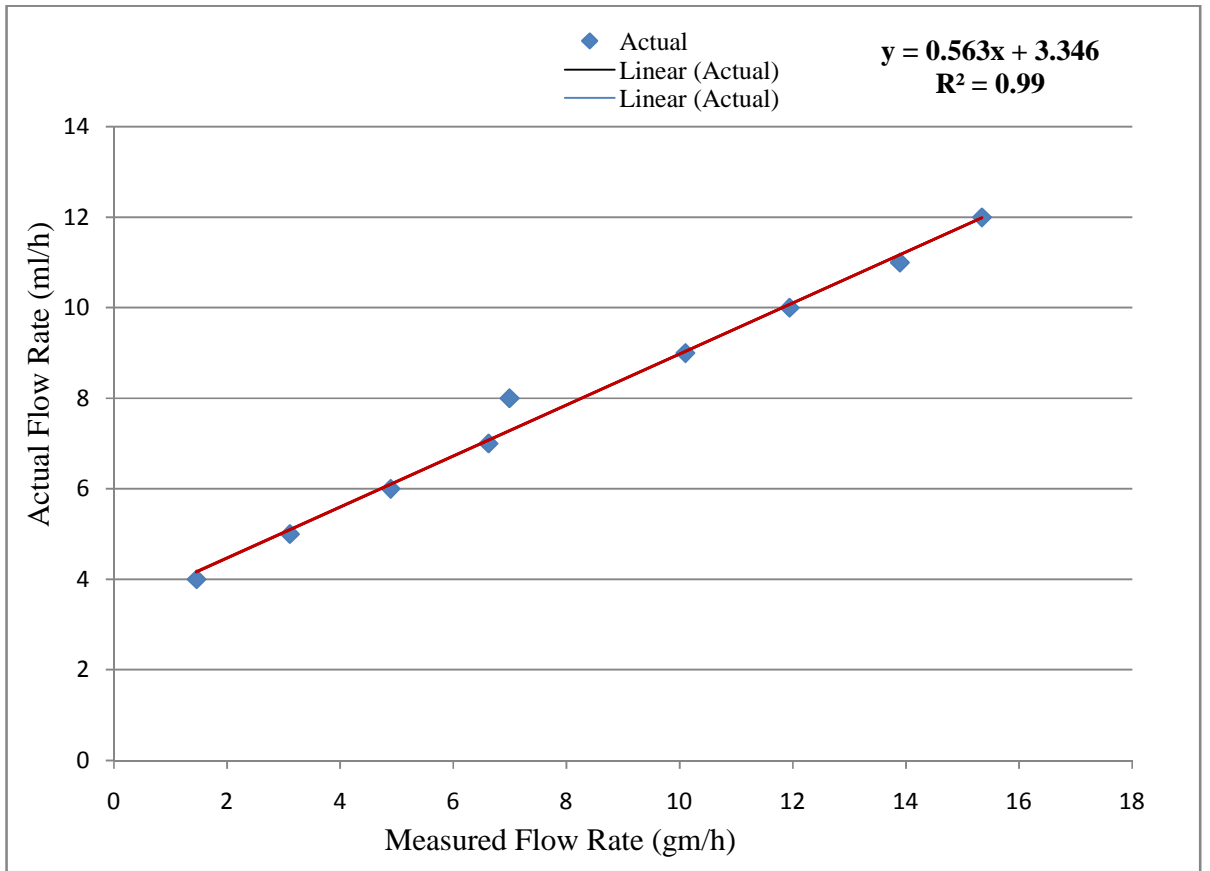


Figure 3.9: Calibration curve for the experiment no. 4

# Chapter 4

## 4.1 Conclusion:

The main objective of this work was to measure and analyze the sap flow rate using the sap flow meter (SGA5) in stem of the virtual plant and the biggest challenge was to simulate the Virtual plant model in which water flowing through stem of the virtual plant model must match exactly as the sap flows in the natural plants. In order to do so, we designed several virtual plant models and also modified the stem several times and along with that we have also taken several measurements. But in this thesis we have particularly talked about only four design of the virtual plant model, in which experiment number 3 and 4 were giving the stable readings as well as satisfactory results for the medium flow rate (i.e., 5 gm/h to 10 gm/h) and for the first two experiments we haven't computed the flow rate because of very bad repeatability of data.

In the experiment 1, the repeatability of the measured data wasn't satisfactory, so we haven't further analyzed the data. So, to test the repeatability of the data we made a little change in the configuration of virtual plant (especially in the stem design to reduce the flow rate to extreme), which lead us to perform another experiment.

In the experiment 2, we have reduced the flow rate to extreme and then we have taken the measurements but unfortunately we didn't get any variation in the thermocouples signals when we were varying the flow rate, so this experiment was also failed and gave us the clue that our system might not be suitable for measuring the extreme low flow rate or the sensor resolution is not good as require to detect extreme low flow rate and this lead us to perform another experiment.

In the experiment 3, our main aim was to reduce the volume (not reducing the flow rate) of the water flowing through the pipe so that the water flowing through the stem of virtual plant model gets more heat in order to get more temperature variation between two thermocouple junctions and fortunately this design worked and this was the first design which gave us satisfactory results but still the design failed to measure the flow rate for more than 9 ml/h. So, to measure the higher flow rate we have again performed another experiment.

In all the earlier experiments the stem was placed horizontally and the sensor was also installed horizontally but in the experiment 4, we have changed the orientation of the pipe (i.e., stem of the virtual plant model) such that the water flowing through the pipe must be in the vertical direction as the sap flows in the natural plant. This experiment hasn't given us any new result and still failed to measure higher flow rate, except excellent repeatability.

Therefore, by looking all the facts and the results we may conclude that the experiment 4 was the best design we have made to measure the flow rate between 6ml/h to 10 ml/h with excellent repeatability and to get the better results for the other flow rates we may have to either change the sensor with the greater stem diameter or we will have to try a completely different virtual plant model.



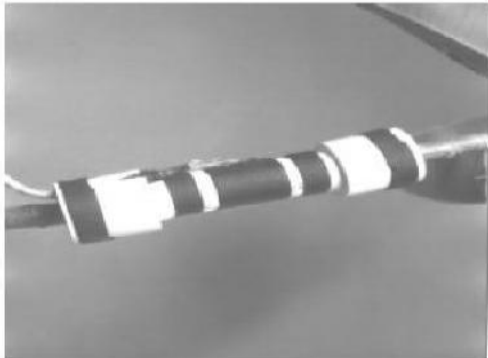





## **4.2 Future scope of the work**

Keeping all the studies carried out in the present work as background, there are a number of areas in which the work can be further explored. A few prospective areas of research can be highlighted as follows:

- The design of the virtual plant model can be further improved to get more accurate results.
- The operating range of the virtual plant model can also be further improved.
- The signals coming from the sensor can be amplified and processed in the LABVIEW to determine and analyze the flow rate automatically and based on this experience a complete signal processing system and a complete PCB can be separately designed.
- With the help of signal processing system the sensor can be used to measure the sap flow rate in any real plant and we can also record the sap flow rate for the reference data.
- Based on the reference data we can design a closed loop feedback system which determines the application of the water from the actual plant use. Thus, we can make the whole irrigation system automatic.
- Since the air quality is an increasing area of concern these days, the effect of the air pollution on the process of photosynthesis and respiration can be indirectly measured via sap flow instrumentation and to overcome these effects appropriate action can be taken accordingly.
- The sensor can also be used to solve potential applications having great benefit to the plant breeding and farming industry. Breeder can observe genetic engineered plants for resistance to drought, growth patterns, water and fertilizer efficiency.

# APPENDIX

## A-1: Dynagage Sensor Installation (with weather shield)

<p>Step5: Instalation- Heater position</p> 	<p>Step1: Sanding, rough or loose bark</p> 
<p>Step6: O-ring Installation</p> 	<p>Step2: Cleaning</p> 
<p>Step7: Install shield over sensor</p> 	<p>Step3: Canola Release spray</p> 
<p>Step8: Sensor shield - Top</p> 	<p>Step4: Heater Position.</p> 





Step 9: secure shield below the sensor



Step 10: Second wrap at cordon 'T' over all wrapping stem below sensor wrapped in thin foil or bubble shield

## A-2: Sensor Maintenance





## References

- [1] Syringe infusion pump LPM-50DN, [www.lifeplusmedical.com](http://www.lifeplusmedical.com)
- [2] Dynamax Inc. 1990. Dynagage Users manual. Houston, TX
- [3] Sakuratani, T.(1981) A heat balance for measuring water flux in the stem of intact plants, *Journal of Agricultural Meteorology*, 37, 9-17
- [4] Sakuranatni, T. (1984) Improvement of the probe for measuring water flow rate in intact plants with the stem heat balance method. *Journal of Agricultural Meteorology*, 40, 273-277
- [5] Baker, J.M. and C.H.M. van Bavel. 1987. Measurement of mass flow of water in stems of herbaceous plants. *Plant, Cell, and Environment* 10: 777-782.
- [6] Baker, J.M., and J.L. Nieber. 1989. An analysis of the steady-state heat balance method for measuring sap flow in plants. *Agric. For. Meteorol.*, 48:93-109.